DOT/FAA/TC-22/31

Federal Aviation Administration
William J. Hughes Technical Center
Aviation Research Division
Atlantic City International Airport
New Jersey 08405

Accounting for Baseline Drift in the Microscale Combustion Calorimeter

September, 2022

Final report

U.S. Department of Transportation
Federal Aviation Administration

NOTICE

This report is available at the Federal Aviation Administration William J. Hughes Technical Center's Full-Text Technical Reports page: actlibrary.tc.faa.gov in Adobe Acrobat portable document format (PDF).

Technical Report Documentation Page

Form DOT F 1700.7 (8-72) Reproduction of completed page authorized

1. Report No.	2. Government Accession No.	3. Recipient's Catalog No.
DOT/FAA/TC-22/31		

4. Title and Subtitle	5. Report Date
Accounting for Baseline Drift in the Microscale Combustion Calorimeter	September, 2022
	6. Performing Organization Code: ANG-211
7. Author(s): Richard E. Lyon, Richard N. Walters, Natallia Safronava, Haiqing Guo	8. Performing Organization Report No.
9. Performing Organization Name and Address: Federal Aviation Administration, William J. Hughes Technical Center, Fire Safety Branch, Atlantic City International Airport, NJ 08405; Diakon Solutions, 110 W Beaver Dr., Cape May Court House, NJ 08210	10. Work Unit No. (TRAIS)
	11. Contract or Grant No.
12. Sponsoring Agency Name and Address: Transport Standards Branch, AIR-670, Policy and Innovation Division, 2200 South 216th Street, Des Moines, Washington	13. Type of Report and Period Covered
	14. Sponsoring Agency Code: AIR-670

15. Supplementary Notes

16. Abstract

The aircraft industry in partnership with the Federal Aviation Administration (FAA) formed a task group in 2013 to consider using the American Society for Testing and Materials (ASTM) D7309 "Standard Test Method for Determining Flammability Characteristics of Plastics and Other Combustible Solid Materials Using Microscale Combustion Calorimetry" (MCC) as an alternate means of complying with 14 CFR 25 flammability regulations when a combustible constituent of a certified cabin construction is changed due to availability, economics, performance, or environmental concerns. A combustible constituent may be an adhesive, potting compound, film, fiber, resin, coating, binder, paint, etc., formulated with a new flame retardant, pigment, etc., that is used in the construction of a cabin material and can be tested in the MCC at the milligram scale. The use of ASTM D7309 for high precision measurements of aircraft cabin materials for regulatory purposes required a level of accuracy and reproducibility that was beyond the capability of the 2013 version of the ASTM D7309 standard when the FAA-Industry task group was formed. At the time, the calculation of the flammability characteristics did not include a correction for baseline drift- which can be a significant source of error for low flammability aircraft cabin materials. The calculation of the calorimeter signal was revised in 2019 to include the effect of combustion gases, which improved the accuracy of the flammability parameters, and was codified as ASTM D7309-19 and later versions. Correction for baseline drift was complicated by random fluctuations of the MCC signal that precluded the subtraction of a pre-recorded background signal, as is routine in thermal analysis. This report describes an analytic approach to baseline correction that is specific to the MCC and can be used to correct the calorimeter signal for temperature-dependent drift during the test to improve the accuracy and reproducibility of MCC flammability parameters of combustible materials.

17. Key Words	18. Distribution Statement
Microscale combustion calorimetry Flammability Fire Growth Capacity Fire Performance	This document is available to the U.S. public through the National Technical Information Service (NTIS), Springfield, Virginia 22161. This document is also available from the Federal Aviation Administration William J. Hughes Technical Center at actlibrary.tc.faa.gov.

19. Security Classif. (of this report)	20. Security Classif. (of this page)	21. No. of Pages	22. Price
Unclassified	Unclassified		

ACKNOWLEDGEMENTS

Please note that certain companies are identified in this paper in order to adequately specify the experimental procedure. This in no way implies endorsement or recommendation by the Federal Aviation Administration.

Contents

Figures

Tables

Acronyms

Acronym	Definition
ASTM	American Society for Testing and Materials
FAA	Federal Aviation Administration
FGC	Fire growth capacity
LOD	Limit of detection
MCC	Microscale combustion calorimetry/calorimeter
PBI	Polybenzimidazole
RMS	Root mean square

Executive summary

The aircraft industry in partnership with the Federal Aviation Administration (FAA) formed a task group in 2013 to consider using ASTM D7309 “Standard Test Method for Determining Flammability Characteristics of Plastics and Other Combustible Solid Materials Using Microscale Combustion Calorimetry” as an alternate means of complying with 14 CFR 25 flammability regulations when a combustible constituent of a certified cabin construction is changed due to availability, economics, performance, or environmental concerns. A combustible constituent may be an adhesive, potting compound, film, fiber, resin, coating, binder, paint, etc., formulated with a new flame retardant, pigment, etc., that is used in the construction of a cabin material and can be tested in the microscale combustion calorimeter (MCC) at the milligram scale. The use of ASTM D7309 for high precision measurements of aircraft cabin materials for regulatory purposes required a level of accuracy and reproducibility that was beyond the capability of the 2013 version of the ASTM D7309 standard when the FAA-Industry task group was formed. At the time, the calculation of the flammability characteristics did not include a correction for baseline drift- which can be a significant source of error for low flammability aircraft cabin materials. The calculation of the calorimeter signal was revised in 2019 to include the effect of combustion gases, which improved the accuracy of the flammability parameters, and was codified as ASTM D7309-19 and later versions. Correction for baseline drift was complicated by random fluctuations of the MCC signal that precluded the subtraction of a pre-recorded background signal, as is routine in thermal analysis. This report describes an analytic approach to baseline correction that is specific to the MCC and can be used to correct the calorimeter signal for temperature-dependent drift during the test to improve the accuracy and reproducibility of MCC flammability parameters of combustible materials.

1 Introduction

In 2013 the aircraft industry in partnership with the Federal Aviation Administration (FAA) began an evaluation of ASTM D7309 “Standard Test Method for Determining Flammability Characteristics of Plastics and Other Combustible Solid Materials Using Microscale Combustion Calorimetry” (ASTM International, 2013) as an alternate means of complying with 14 CFR 25 flammability regulations when a combustible constituent of a certified construction must be substituted due to unavailability, economic reasons, performance considerations, or environmental concerns. Combustible constituents of stowage bins, sidewall panels, bulkheads, partitions, insulation blankets, and molded parts include adhesives, potting compounds, films, fibers, resins, coatings etc. that can be tested at the 10 mg scale in a microscale combustion calorimeter (MCC). Figure 1 is a schematic diagram of the MCC. In the MCC test, solid samples are thermally decomposed at constant heating rate and the pyrolysis gases are combusted in excess oxygen. The specific heat release rate Q is computed from the mass flow rate of oxygen in the evolved combustion gases measured at an external chemical oxygen sensor.

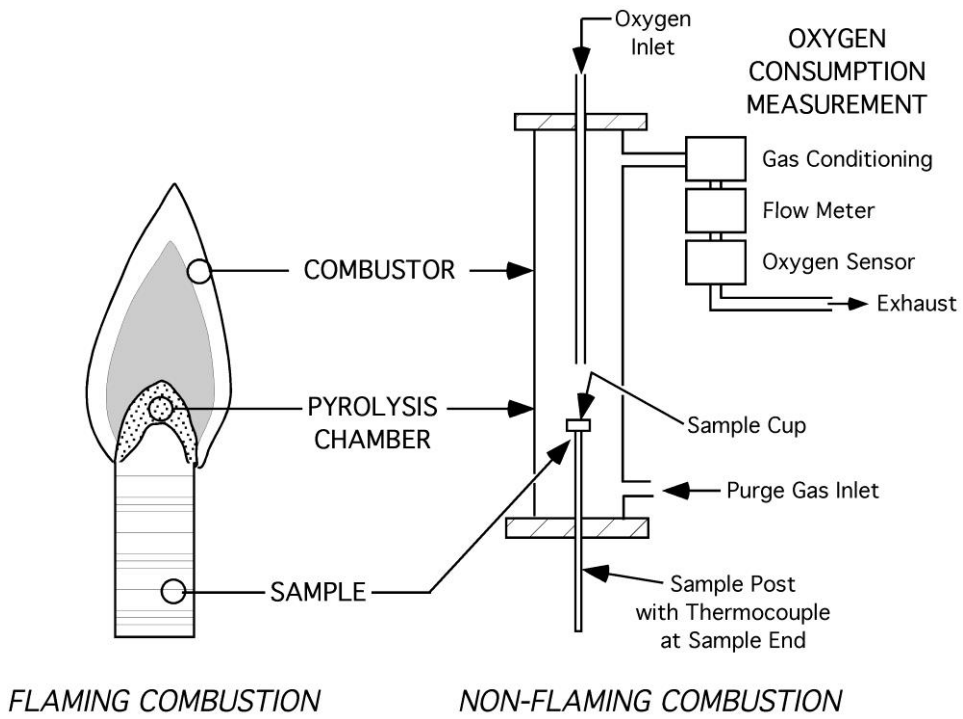

Figure 1. Schematic diagram of the microscale combustion calorimeter

The ability of the MCC to resolve small differences in combustion characteristics of certified and substitute materials requires a level of accuracy and reproducibility that was unavailable using

the 2013 version of the ASTM standard D7309-13 (ASTM International, 2013). In 2017, the effect of combustion gases on the oxygen sensor and flow meter outputs was determined (Guo, Lyon, & Safronava, 2017) and incorporated into the revised calculation of the time (t) and temperature (T) dependent calorimeter signal $q(t,T)$ in ASTM D7309-19 (ASTM International, 2019) and in more recent versions of the standard (ASTM International, 2021). However, it was unclear whether the updated $q(t,T)$ calculation (ASTM International, 2019; ASTM International, 2021) in the absence of a sample (i.e., the instrument baseline, q^0) could be recorded and subtracted from test data to correct for baseline drift, as is routinely done in other methods of constant heating rate thermal analysis (Gibson, Simmons, Stittt, Horsburgh, & Gallen, 2022; ASTM International, 2018; ASTM International, 2021). For commodity plastics such as polyethylene, nylon and polyester, the change in the instrument baseline q^0 is a small fraction of the sample response Q, but it can be a significant fraction for low flammability plastics used in the construction of aircraft interiors, as illustrated in Figure 2.

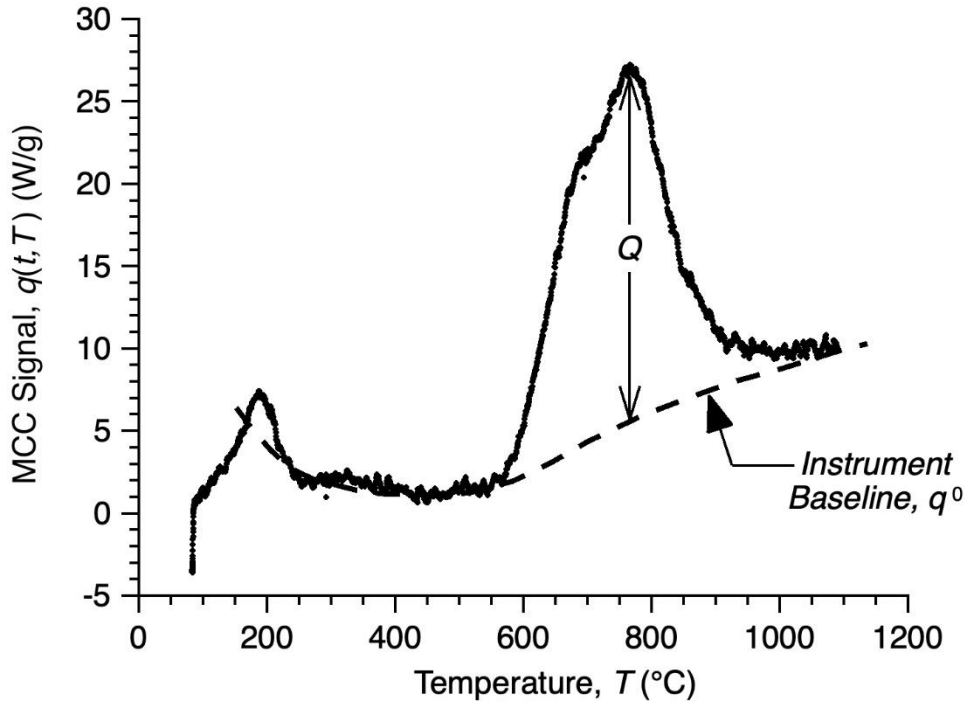

Figure 2. Components of MCC signal for polybenzimidazole

In this report, the MCC thermal baseline q_0 is derived and extended to ASTM D7309-19 (ASTM International, 2019) and later (ASTM International, 2021) versions of the standard (ASTM D7309-19+) containing the new $q(t,T)$ calculation. The thermal baseline q_0 is compared to the instrument baseline q^0 for different experimental endpoints (global and local) and pyrolysis environments (anaerobic, aerobic).

Recently, a MCC parameter that includes both ignitability and heat release components of fire growth was identified and called the fire growth capacity (FGC) (Lyon, Safronava, Crowley, & Walters, 2021; Lyon, Safronava, Crowley, & Walters, 2020; Safronava, Lyon, & Walters, 2020). It was shown through testing that the FGC could be used to compare the intrinsic flammability of materials in general (Lyon, Safronava, Crowley, & Walters, 2021), and the constituents of aircraft cabin constructions, in particular (Lyon, Safronava, Crowley, & Walters, 2020; Safronava, Lyon, & Walters, 2020). However, in order to compare materials for FAA regulatory purposes using FGC, it is necessary to obtain accurate and reproducible heat release temperatures and heats of combustion of aircraft materials. The effect of the different baseline correction methods on the specific heat release, h_c, and the FGC, measured in ASTM D7309-19+ is included in this report.

2 ASTM D7309-13

The physical construction and standard operation of the microscale combustion calorimeter according to the ASTM D7309 (ASTM International, 2013; ASTM International, 2019; ASTM International, 2021; Lyon, Walters, Stoliarov, & Safronava, 2014) results in transient gas composition and flow rate gradients. There is a small but measurable change in the zero-point value (baseline) of the calorimeter signal q^0 underlying the specific heat release rate $Q(t)$ of combustible materials as illustrated in Figure 2. The temperature dependence of this baseline drift is the subject of the following sections.

2.1 Calorimeter signal

The 2013 version of ASTM D 7309 (ASTM International, 2013) computes a calorimeter signal $q(t,T)$ at time t and temperature T during transient heating, using a volumetric balance of the combustion gases according to Equation 1.

$$q(t,T) = \frac{E\rho_{O_2}}{m_0} F\left(X^0_{O_2} - X_{O_2}\right) \tag{1}$$

In Equation 1, $F = F(t)$ is the instantaneous volumetric flow rate, $X_{O_2} = X_{O_2}(t)$ is the oxygen concentration (mole fraction) of the combustion stream exiting the MCC at standard (room) temperature 298K (25°C), and $X^0_{O_2}$ is the initial oxygen mole (volume) fraction prior to the start of the test. As the temperature of the pyrolyzer of volume V_p increases at a constant rate, $\beta = dT/dt$, the terminal flow rate changes slightly in accordance with the ideal gas law (Lyon, Walters, Stoliarov, & Safronava, 2014).

$$F(t) = F_{N_2} + F_{O_2} + \beta V_p/T \tag{2}$$

Standard values of the parameters in Equation 1 and Equation 2 are listed in Table 1 (Lyon, Walters, Stoliarov, & Safronava, 2014).

2.2 Thermal baseline for anaerobic pyrolysis (Method A)

In Method A of ASTM D7309, a milligram sample is inserted into the pyrolyzer, which is purged with a constant volumetric flow of nitrogen, F_{N_2} (cm^3/min) measured at standard temperature (298K) and pressure (1 Bar). The nitrogen sweeps the volatile thermal decomposition products from the pyrolyzer and mixes them with a constant volumetric flow of oxygen F_{O_2} in the combustor. During a test, the temperature of the sample/pyrolyzer is increased at a constant rate, $dT/dt = \beta$ = 1K/s (typically), which increases the volumetric flow rate at the terminal flow meter in accordance with Equation 2. During the heating period, there is a corresponding decrease in the volume (mole) fraction of oxygen at the sensor in accordance with,

$$X_{O_2}(t) = \frac{F_{O_2}}{F(t)} \pm \delta X_{O_2} \approx \frac{F_{O_2}}{F(t)} \tag{3}$$

In Equation 3, δX_{O_2} is the random fluctuation in the X_{O_2} reading of the terminal oxygen sensor, which is typically on the order of $\pm 10^{-4}$ m^3-O_2/m^3 and can be neglected in comparison to $F_{O_2}/F(t) \approx 0.2$ for Method A. Differential heating of the N_2 entering pyrolyzer at temperature T relative to the constant flow of O_2 into the combustor at constant temperature T_c generates a time-dependent N_2/O_2 gradient at the terminal flow meter and oxygen sensor. In the absence of oxygen consumption due to combustion, the terminal flow rate at pyrolyzer temperature T during heating from an initial temperature T_0 to a final (≈ combustor) temperature $T_\infty \approx T_c$ =1173K (900°C) is (Lyon, Walters, Stoliarov, & Safronava, 2014),

$$F(T) = F^0 + \beta V_p \left(\frac{1}{T} - \frac{1}{T_c}\right) \tag{4}$$

Since, $F(T_0) = F(T_\infty) = F^0$ at $\beta = 0$ when measured at standard temperature and pressure,

$$X_{O_2}^0 = F_{O_2}/F^0 = F_{O_2}/F(T_\infty) \tag{5}$$

Substituting Equation 3 and Equation 4 into Equation 1, gives the zero-point value of the calorimeter signal at temperature T in the absence of a sample (i.e., the thermal baseline) for Method A of the 2013 (ASTM International, 2013) version of the standard,

$$q_0(T) = \frac{E\rho_{O_2} X_{O_2}^0 \beta V_p}{m_0}\left(\frac{1}{T} - \frac{1}{T_c}\right) \tag{6}$$

The Method A thermal baseline in ASTM D7309-13 (ASTM International, 2013) Equation 6 can be described by two constants, $C_{1\text{-A13}}$ and $C_{2\text{-A13}}$, and the sample/pyrolyzer temperature T,

$$q_0(T) = \frac{E\rho_{O_2}X_{O_2}^0\beta V_p/m_0}{T} - \frac{E\rho_{O_2}X_{O_2}^0\beta V_p/m_0}{T_c} = \frac{C_{1-A13}}{T} - C_{2-A13} \quad (7)$$

The baseline coefficients in Equation 7 can be computed for standard values of the constituent parameters listed in Table 1: $C_{1\text{-A13}}$ = 5450 W-K/g and $C_{2\text{-A13}}$ = 4.65 W/g. The magnitude of the baseline drift using these coefficients for a spurious 5 mg sample heated from T_0 = 323K (50°C) to $T_\infty = T_c$ = 1273K (1000°C) at β = 1K/s during the normal operation of the instrument is: $\Delta q_0 = q_0(T_\infty) - q_0(T_0) \approx 10$ W/g. This value is compared to experimental data for the same spurious 5 mg sample in Figure 7 for two different oxygen sensors.

Table 1. Nominal values of the parameters in Equations 1-12

Parameter	**Symbol**	**Standard Value**
Heat of combustion of oxygen with typical organic fuels	E	13.1 MJ/kg-O_2
Density of oxygen at 25°C	ρ_{O_2}	1.3 kg/m^3
Initial/final O2 mole (volume) fraction	$X_{O_2}^0$	0.2
Pyrolyzer volume	V_p	8 x 10^{-6} m^3
Pyrolyzer/Sample Heating rate	β	1 K/s
Initial sample mass	m_0	5 x 10^{-6} kg
Initial sample (pyrolyzer) temperature	T_0	323K (50°C)
Final sample (combustor) temperature	T_∞	1173K (900°C)

2.3 Thermal baseline for oxidative pyrolysis (Method B)

In Method B of ASTM D7309, a constant flow of nitrogen (F_{N_2}) and oxygen (F_{O_2}) are mixed prior to entering the pyrolyzer. In the absence of oxygen consumption by combustion, the mole fraction of oxygen X_{O_2} measured at the terminal oxygen sensor under ambient conditions should be unchanged from the initial value $X_{O_2}^0$. Consequently, oxygen sensor fluctuations δX_{O_2} become significant during the heating period. The terminal flow rate $F(T)$ increases during the heating period in accordance with Equation 2, so the zero-point value of the calorimeter signal (thermal baseline) during pyrolyzer heating at constant heating rate dT/dt = β in the absence of a sample is,

$$q_0(T) = \frac{E\rho_{O_2}}{m_0}F(t)\left[X_{O_2}^0 - \left(X_{O_2}^0 + \delta X_{O_2}\right)\right] = -\frac{E\rho_{O_2}\beta V_p\,\delta X_{O_2}}{m_0}\left(\frac{1}{T} - \frac{1}{T_c}\right) = \frac{C_{1-B13}}{T} - C_{2-B13} \quad (8)$$

The thermal baseline for Method B of ASTM D7309-13 (Equation 8) has the same form as Method A (Equation 7), except that the baseline coefficients are opposite in sign,

$$C_{1-B13} = -\frac{E\rho_{O_2}\beta V_p}{m_0},$$

$$C_{2-B13} = -\frac{E\rho_{O_2}}{m_0}\left[F^0 - \frac{\beta V_p}{T_c}\right]\delta X_{O_2} \approx -\frac{E\rho_{O_2}}{m_0}\delta X_{O_2}$$

3 ASTM D7309-19 and later versions

3.1 Calorimeter signal

The revision of D7309-13 (ASTM International, 2013), first adopted by ASTM in May 2019 (ASTM International, 2019) and persisting through the 2021 version (ASTM International, 2021), accounts for carbon dioxide generated by complete combustion of the hydrocarbon fuel gases. Carbon dioxide affects the volumetric flow rate and the output of the terminal flow meter in both Method A and Method B of the standard procedure (Guo, Lyon, & Safronava, 2017). The calorimeter signal in ASTM D7309-19 is calculated from a mass balance on oxygen using the terminal flow rate measured prior to the start of the transient heating experiment, $F^0 = F_{O_2} + F_{N_2}$,

$$q(t,T) = \frac{E\rho_{O_2}}{m_0}\left\{F^0 X^0_{O_2} - F X_{O_2}\left[1 - \frac{1}{3}\left(X^0_{O_2} - X_{O_2}\right)\right]\right\} \quad (9)$$

In Equation 9, as previously, $F = F(T)$ is the terminal flow rate at pyrolyzer temperature T and $X_{O_2} = X_{O_2}(t)$ is the oxygen concentration (mole fraction) in the combustion stream, during an increase in the pyrolyzer (sample) temperature from T_0 to T_∞ at constant heating rate, β(K/s).

3.2 Thermal baseline for anaerobic pyrolysis (Method A)

In the absence of a sample, the zero-point value of the calorimeter signal $q_0(T)$ changes with temperature T because of thermal expansion of the pyrolyzer purge gas into the combustor at constant heating rate $dT/dt = \beta$. Using the previous definitions and substitutions in Equation 9, and assuming $\delta X_{O_2}/X_{O_2} << 1$, the thermal baseline is,

$$q_0(T) = \frac{E\rho_{O_2}\left(X^0_{O_2}\right)^2 \beta V_p/3m_0}{T} - \frac{E\rho_{O_2}\left(X^0_{O_2}\right)^2}{3m_0 T_c/\beta V_p} = \frac{C_{1-A19}}{T} - C_{2-A19} \quad (10)$$

Equation 10 is the thermal baseline of the calorimeter during normal operation in accordance with Method A of ASTM D7309-19 (ASTM International, 2019) and later versions (ASTM International, 2021). Equation 10 has the same reciprocal temperature dependence as Equation 7

of ASTM D7309-13, but the coefficients C1-A19 and C2-A19 of Equation 10 are ten times smaller than C1-A13 and C2-A13 of Equation 7. This is due to the $(X_{O_2}^0)^2$ term arising from the more accurate oxygen mass balance (Equation 10) compared to the oxygen volume balance (Equation 7), so the curvature of q_0 in ASTM D7309-19 (Method A) (ASTM International, 2019; ASTM International, 2021) is correspondingly reduced.

Standard coefficients of ASTM D7309-19 (Guo, Lyon, & Safronava, 2017) baseline drift for a spurious 5 mg sample at typical $X_{O_2}^0$ = 0.2 and $T_\infty = T_c$ = 1173K (900°C) are, $C_{1\text{-A19}}$ = 363 W-K/g and $C_{2\text{-A19}}$ = 0.31 W/g using the nominal parameters in Table 1. The magnitude of the baseline drift for a spurious 5 mg sample between T_0 = 323K and T_∞ = 1173K during normal operation of the commercial instrument, is estimated to be of the order, $\Delta q_0 = q_0(T_0) - q_0(T_\infty) \approx 1$ W/g, using these coefficients in Equation 10, as illustrated in Figure 8A.

3.3 Thermal baseline for oxidative pyrolysis (Method B)

In Method B of ASTM D7309-19 (ASTM International, 2019; ASTM International, 2021), the nitrogen and oxygen are mixed prior to entering the pyrolyzer and heated at the same constant rate, β(K/s) as per D7309-13 (ASTM International, 2013). There is no differential expansion of N_2 relative to O_2 that would cause an N_2/O_2 gradient at the terminal O_2 sensor in the absence of combustion. However, the terminal flow rate $F(T)$ increases during the heating period as per Equation 4. In the absence of combustion, and with $\delta X_{O_2}/ X_{O_2}^0 << 1$, Equation 9 gives the zero-point value of $q(t)$ when $X_{O_2} \approx X_{O_2}^0$,

$$q_0(T) = \frac{E\rho_{O_2} X_{O_2}^0}{m_0}(F^0 - F(t)) \tag{11}$$

Substituting Equation 4 into Equation 11 with $F(T_0) = F(T_\infty) = F^0$ shows that the thermal baseline for Method B of ASTM D7309-19 has the same form as the thermal baseline of Method A of ASTM D7309-13 (Equation 7),

$$q_0(T) = \frac{E\rho_{O_2} X_{O_2}^0 \beta V_p/3}{m_0}\left\{\frac{1}{T} - \frac{1}{T_c}\right\} = \frac{C_{1-B19}}{T} - C_{2-B19} \tag{12}$$

4 Experiment

4.1 Materials

The polystyrenes (PS) used in these studies were general purpose, food grade, crystal-clear bulk polymers prepared by free radical polymerization. It has been shown (Lyon, Walters, Stoliarov, & Safronava, 2014) that any crystal clear, atactic polystyrene obtained by free radical

polymerization is similar in chemical structure and will produce similar results when tested in the MCC. Three (3) to five (5) replicate tests of specific heat release h_c and FGC were conducted for each of the polystyrenes on multiple dates over a period of years. Likewise, replicate tests of three hundred (300) thermosetting polymers and thermoplastics of known and unknown composition used in commercial air transport, military aircraft, automotive applications, home furnishings, and transportation were tested over a period of years. Ultra-high purity (> 99.99%) oxygen and nitrogen for MCC experiments were obtained from local distributors.

4.2 Methods

All tests were conducted by expert users on site-built MCCs conforming to ASTM D7309-21 and using the chemical oxygen sensor supplied with commercial instruments (Automotive Oxygen Sensor, R17A, Teledyne Analytical Instruments, City of Industry, CA 91748), unless otherwise noted. Tests to measure the thermal baseline q^0 using empty sample pans were scaled to a typical q range by assuming a spurious sample mass of 5 mg. This scaling of q^0 does not suggest or recommend the use of 5 mg samples if they do not conform to the heating rate limitations of ASTM D7309-19+. A limited number of empty pan baseline measurements were conducted using a paramagnetic oxygen analyzer (Pm1111E, Hummingbird Sensing Technology, East Sussex, UK) to determine the effect of oxygen sensor baseline stability on q^0.

4.2.1 Anaerobic pyrolysis (Method A)

Experiments were conducted in a microscale combustion calorimeter according to ASTM D7309-13 (ASTM International, 2013) and ASTM D7309-19 (ASTM International, 2019; ASTM International, 2021) Method A (anaerobic pyrolysis) of the standard procedure. In Method A, the pyrolyzer/sample is purged with nitrogen at 80 cm^3/min and heated at a constant rate of β = 1 K/s over the temperature range 323K (50°C) to 1273K (1000°C). Oxygen is supplied to the combustor at a rate of 20 cm^3/min where it combines with the fuel gases in N_2 during the thermal event. Prior to the start of the test, the oxygen concentration is $X_{O_2}^0$ = 0.2 (20 volume percent O_2, balance N_2) and the total flow rate is $F^0 = F_{O_2} + F_{N_2}$= 1.667 x 10^{-6} m^3/s (100 cm^3/min).

4.2.2 Oxidative pyrolysis (Method B)

Experiments were conducted in a microscale combustion calorimeter according ASTM D7309-13 (ASTM International, 2013) and ASTM D7309-19 (ASTM International, 2019; ASTM International, 2021), Method B (oxidative pyrolysis) of the standard procedure. In Method B, the pyrolyzer is purged with synthetic air (20 cm^3/min O_2 + 80 cm^3 /min N_2) for the duration of the

test. Prior to the start of the test, the oxygen concentration is $X_{O_2}^0$ = 0.2 (20 volume percent O_2, balance N_2) and the total flow rate is $F^0 = F_{O_2} + F_{N_2}$= 1.667 x 10^{-6} m^3/s (100 cm^3/min).

4.3 Correcting the calorimeter signal for baseline drift

The specific heat release rate of the sample $Q(t)$ is not exactly equal to the time- and temperature-dependent calorimeter signal $q(t,T)$ because the latter includes the instrument baseline q^0 which is approximated by the thermal baselines q_0 of Equations 6, 8, 10, and 12. In these equations, the thermal baseline coefficients C_1 and C_2 depend on the sample mass and heating rate. Consequently, these baseline coefficients must be computed for each test from the $q(t,T)$ history in the range of temperatures where the heating rate is constant. It has been found that sampling noise is effectively removed from the calorimeter signal $q(t,T)$ and temperature derivative dT/dt using a moving average of 20K/β seconds.

4.3.1 Specific heat release rate

The total differential of the enthalpy (heat) released h(J/g) during transient heating in the MCC at constant pressure is,

$$dh = \left(\frac{\partial h}{\partial T}\right)_t dT + \left(\frac{\partial h}{\partial t}\right)_T dt \tag{13}$$

If the heating rate is constant, $dT/dt = \beta$, the time and temperature dependence of the calorimeter signal can be separated,

$$q(t,T) = \frac{dh}{dt} = \beta\left(\frac{\partial h}{\partial T}\right)_t + \left(\frac{\partial h}{\partial t}\right)_T = Q(t) + q_0(T) \tag{14}$$

Equation 14 is the basis for correcting the time- and temperature-dependent calorimeter signal for thermal drift to obtain the specific heat release rate,

$$Q(t) = q(t,T) - q_0(T) \tag{15}$$

4.3.2 Global baseline correction

4.3.2.1 Reciprocal temperature thermal (1/T) model

Equations 6, 8, 10, and 12 show that the temperature dependence of the reciprocal temperature thermal baselines has the same general form for Method A and Method B of ASTM D7309-13 (ASTM International, 2013) and ASTM D7309-19 (ASTM International, 2019; ASTM International, 2021).

$$q_0(T) \equiv q_0(1/T) = \frac{C_1}{T} - C_2 \tag{16}$$

The thermal baseline coefficients C_1 and C_2 of Equation 16 depend on the sample mass and heating rate (see Equations 6, 8,10, and 12), so they are not universal and must be computed for each test using the coordinates of two points, $p_1 = \{T_1, q_1\}$ and $p_2 = \{T_2, q_2\}$, in the range of temperatures of controlled (constant) heating rate so that Equation 16 applies,

$$C_1 = \frac{T_1 T_2 (q_1 - q_2)}{T_1 - T_2} \qquad \text{(W-K/g)} \tag{17}$$

$$C_2 = \frac{q_1 T_1 - q_2 T_2}{T_2 - T_1} \qquad \text{(W/g)} \tag{18}$$

Figure 3 shows a smoothed calorimeter signal, $q(t,T)$ for a phenolic resin and the thermal baseline $q_0(1/T)$ as an approximation of q^0 between the temperature limits of controlled heating, p_1, p_2.

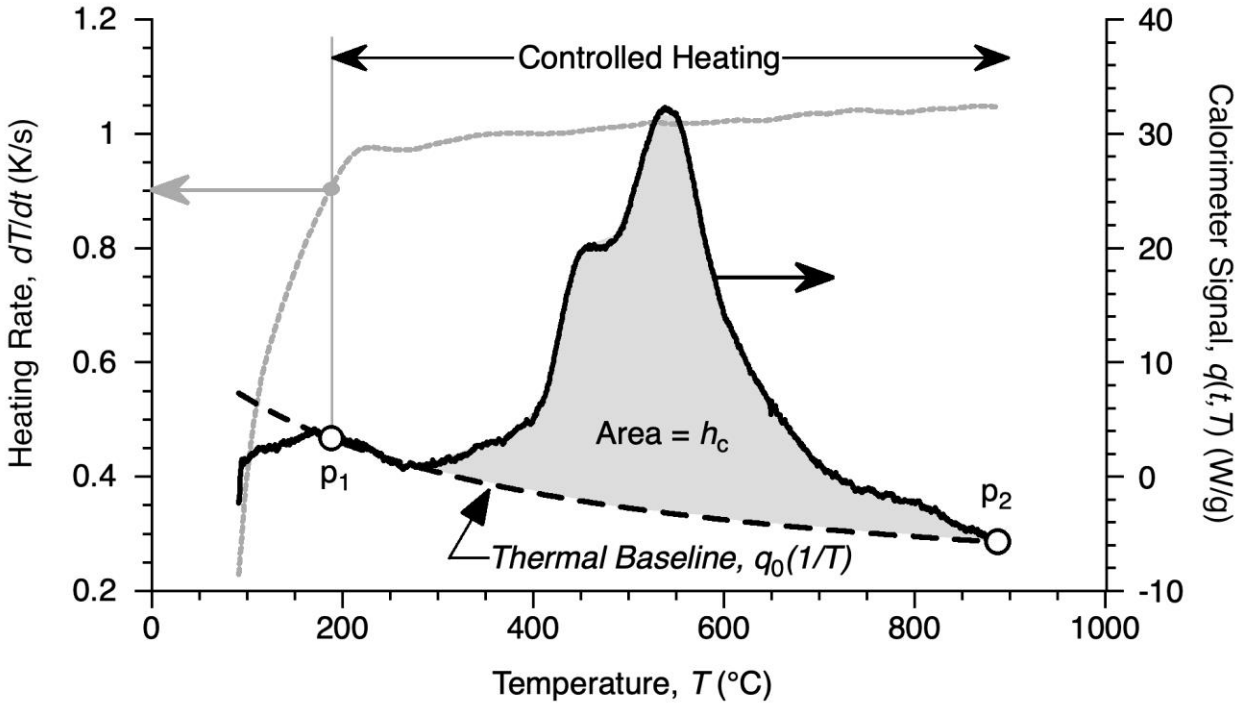

Figure 3. Global baseline correction using Equations 15-16 for β = 1 K/s

4.3.2.2 Linear temperature thermal (T) model

In the absence of specific knowledge of the underlying baseline in thermal analysis, a linear interpolation between the endpoints of a thermal event is recommended (Gibson, Simmons,

Stittt, Horsburgh, & Gallen, 2022). The baseline which linearly interpolates between points, $p_1 = \{T_1, q_1\}$ and $p_2 = \{T_2, q_2\}$, within the limits of controlled heating is,

$$q_0(T) = c_1 + c_2(T - T_1) \tag{19}$$

With,

$$c_1 = q_1, \quad c_2 = \frac{q_2 - q_1}{T_2 - T_1} \tag{20}$$

Multi-point baseline fits to approximate q^0 during the heat release event include polynomial or sigmoidal forms (Gibson, Simmons, Stittt, Horsburgh, & Gallen, 2022), but these are non-physical for MCC and require significant user discretion in selecting the range of data used to evaluate the coefficients. Figure 4 shows the specific heat release rate of the sample $Q(t)$ after correcting for thermal drift (Figure 3) over the region of constant heating. Specific heat release h_c is time integral of $Q(t)$ between the times corresponding to T_1 and T_2 at the first and last minima of $\Delta q(t,T)$.

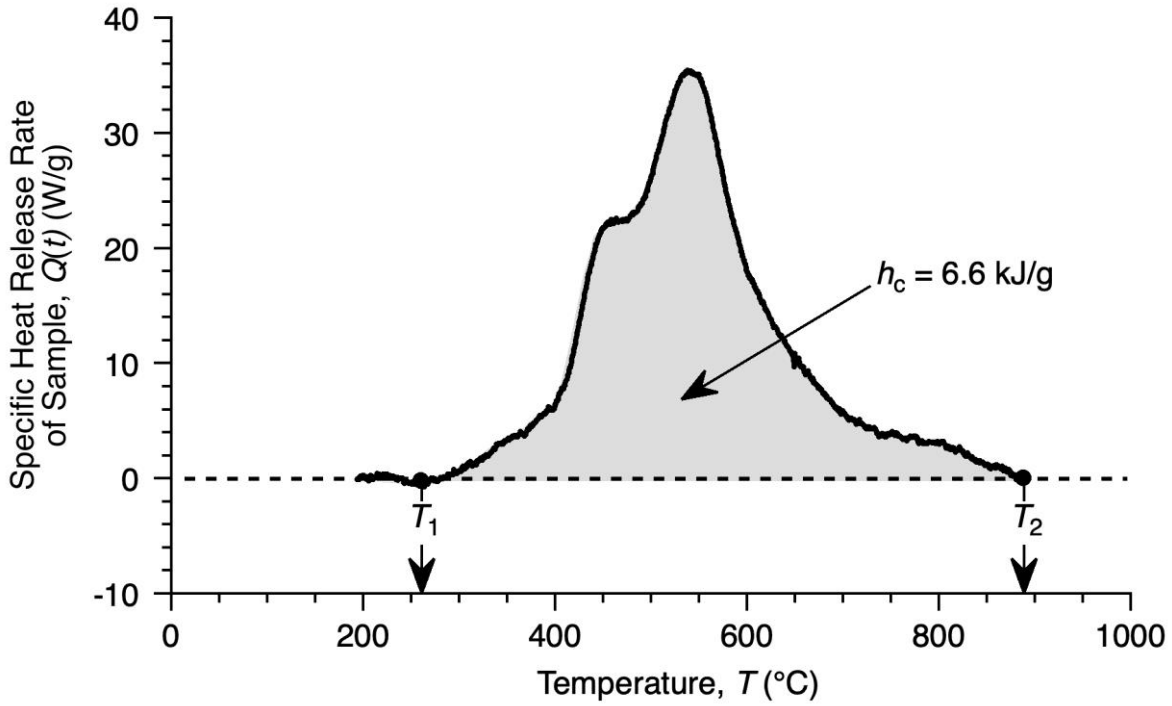

Figure 4. Specific heat release rate of sample $Q(t)$ after correcting for thermal drift

4.3.3 Local baseline correction

Two points, $p_1 = \{T_1, q_1\}$ and $p_2 = \{T_2, q_2\}$, are chosen at the limits of heat release by inspection of the local q history within the global temperature range of controlled heating. In the local

method, the point $p_1 = \{T_1, q_1\}$ is the point of first departure of $q(T)$ from the perceived baseline q^0 (i.e., it is the start of heat release). The point $p_2 = \{T_2, q_2\}$ is the point at which $q(T)$ first returns to the perceived baseline q^0 (i.e., it is the end of heat release). These points, p_1 and p_2, are obtained by visual or numerical inspection of $q(t)$ or algorithmically as the first and last minima in $q(t)$. After p_1 and p_2 are selected, 2-point options for approximating q^0 are the thermal baseline $q^0(1/T)$ of Equation 16, and the linear baseline $q_0(T)$ of Equation 19. Multi-point baseline fits to approximate q^0 during the heat release event include polynomial or sigmoidal forms (Gibson, Simmons, Stittt, Horsburgh, & Gallen, 2022), but these are non-physical for MCC and require significant user discretion in selecting the range of data used to evaluate the coefficients.

4.3.4 Global vs local baseline correction

Figure 5 shows the MCC signal, $q(t,T) = Q(t) + q^0(T)$ for a heat resistant polymer, polybenzimidazole (PBI) in Method A of ASTM D7309-19+. The global linear (T) and thermal ($1/T$) baselines were computed between p_1 and p_2 at the limits of controlled heating. A significant portion of the $q(t,T)$ data fall below the global baselines resulting in negative values of $Q(t)$ after subtraction of $q_0(T)$. In this case, a linear local baseline between p_1 and p_2 may be more appropriate, as indicated by the dotted line in Figure 5. The legend in Figure 5 displays the specific heat release h_c for each baseline range and model, which is the time integral of $Q(t) = q(t,T) - q_0(T)$. It is seen that the specific heat release ranges from $h_c = 2.1$ to $h_c = 4.3$ kJ/g, depending on the method of baseline correction. These values are near the limit of detection of h_c (Section 6.2.2) and the difference is within the uncertainty of h_c (Table 4).

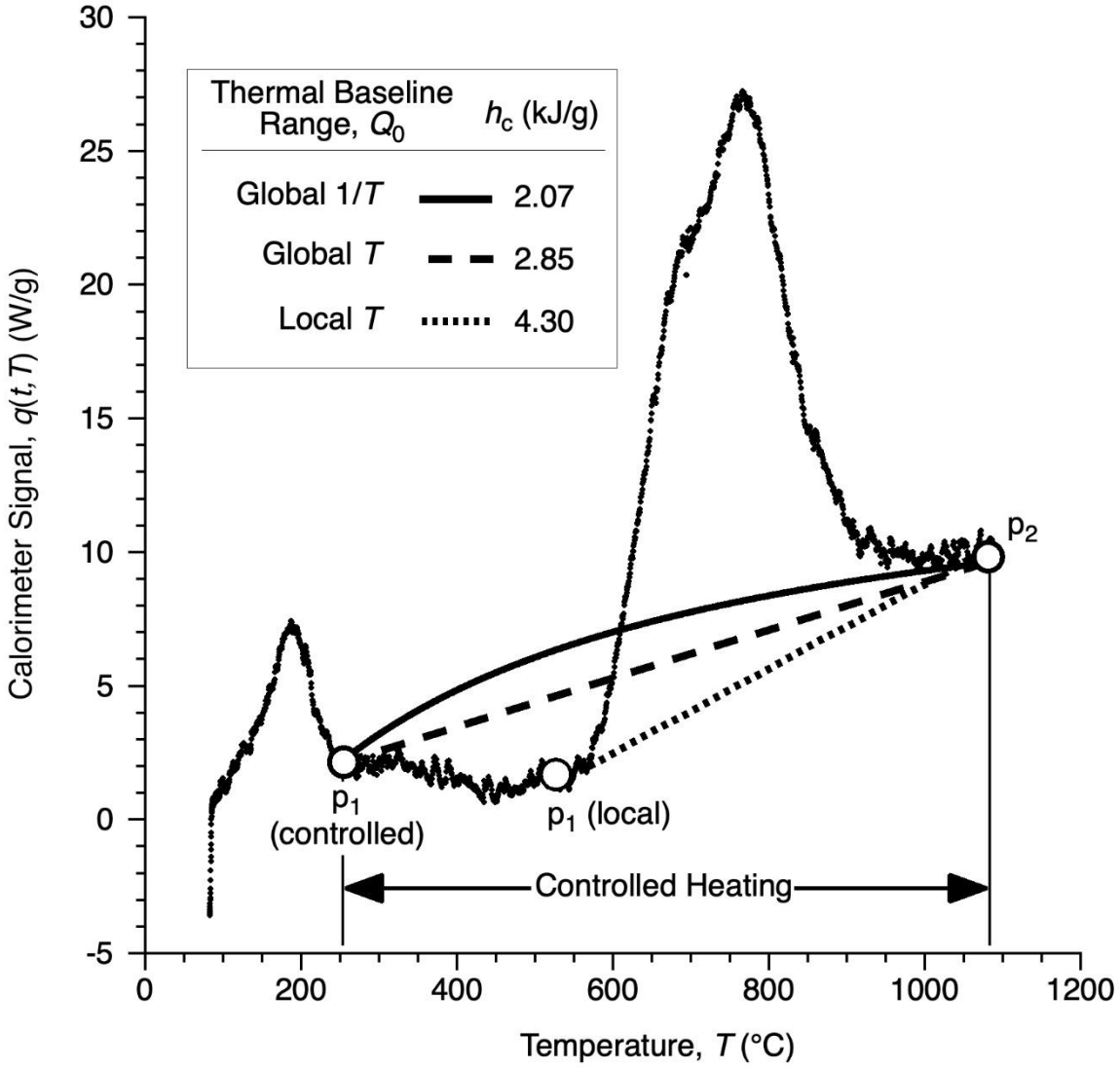

Figure 5. Global and local baselines for polybenzimidazole in Method A of ASTM D7309-19+

4.3.5 Global and local baseline correction

The discrepancy in h_c resulting from exclusive application of the local (Equation 16) or global (Equation 19) baseline corrections in Figure 5 can be mitigated by successive application of the global and local baseline corrections to the same data. In this approach, $q_0(1/T)$ between the temperature limits of controlled heating is subtracted from the calorimeter signal $q(t,T)$ to correct for global thermal drift, $\Delta q(t,T)$. In a subsequent step, a local $q_0(T)$ is subtracted from the global $\Delta q(t,T)$ using a linear baseline between the start, $p_1 = \{\Delta q_1, T_1\}$ and end, $p_2 = \{\Delta q_2, T_2\}$ of heat release to obtain $Q(t) = \Delta q(t,T) - q_0(T)$. Figure 6 illustrates the 2-step global/local baseline correction procedure for the polybenzimidazole data of Figure 5.

5 Results and discussion

5.1 Direct measurement of baseline using empty sample pans

Replicate empty pan measurements of the calorimeter signal, in the absence of a sample or thermal event, q^0, were conducted for Method A and Method B of ASTM D7309-13 and -19. A spurious/virtual sample mass of 5 mg was used to scale q^0 to a typical range of $q(t,T)$. This arbitrary scaling does not suggest or recommend the use of 5 mg samples that do not conform to the heating rate limitations of ASTM D7309. The purpose of these measurements was to determine if a blank experiment (i.e., the instrument baseline) could be recorded and subtracted from subsequent sample experiments to correct for baseline drift during the test, as is routinely done in other constant heating rate thermal analyses such as differential scanning calorimetry (DSC) (ASTM International, 2021) and thermogravimetric analysis (TGA) (ASTM International, 2018). All q_0 calculations were performed in International Standard (SI) units (m, kg, s, K) but are reported in CGS units (cm, g, s, °C) to conform to laboratory thermal analysis convention (ASTM International, 2021; ASTM International, 2018).

Figure 7 shows 10 replicate blank experiments of the instrument baseline q^0 in Method A of ASTM D7309-13 (ASTM International, 2013). The oxygen concentration at the terminal flow meter was measured using a chemical oxygen sensor (A) or a paramagnetic oxygen analyzer (B) to compare the effects of oxygen sensor stability on the instrument baseline. Also shown in Figure 7 as a thick dashed curve, is the thermal baseline in ASTM D7309-13 (ASTM International, 2013) computed from Equation 7 using the properties in Table 1. Figure 7A shows blank tests (instrument baselines) in Method A of ASTM D7309-13, measured using the chemical oxygen sensor supplied with commercial instruments. Figure 7B shows Method A baselines measured under the same standard operating conditions using a paramagnetic oxygen analyzer. It is clear that random baseline fluctuations of the chemical sensor are superimposed on the thermal baseline, and that these are reduced for the paramagnetic oxygen analyzer, although a monotonic thermal baseline drift is evident.

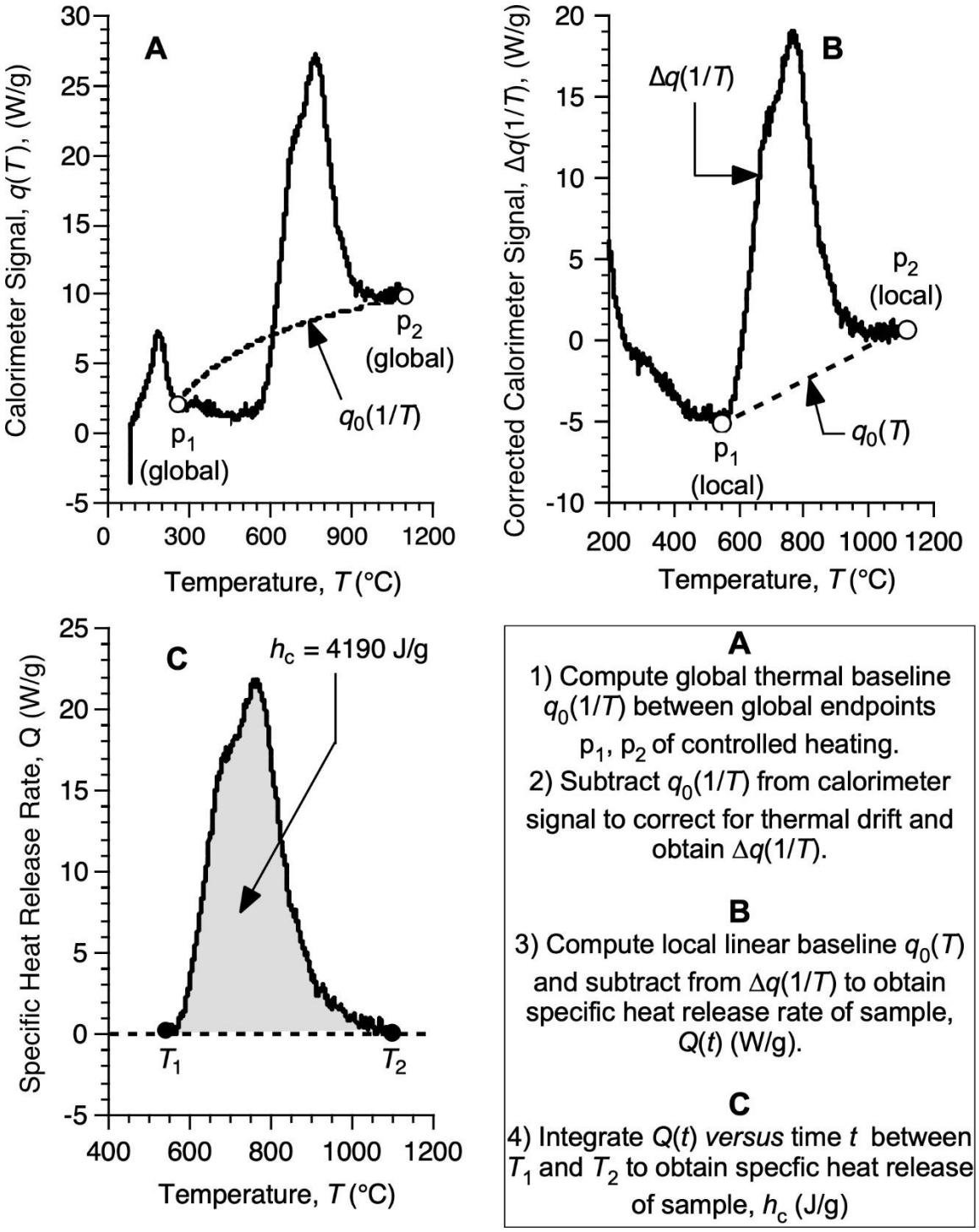

Figure 6. Illustration of 2-step global/local baseline correction procedure

5.1.1 Anaerobic pyrolysis baselines (Method A)

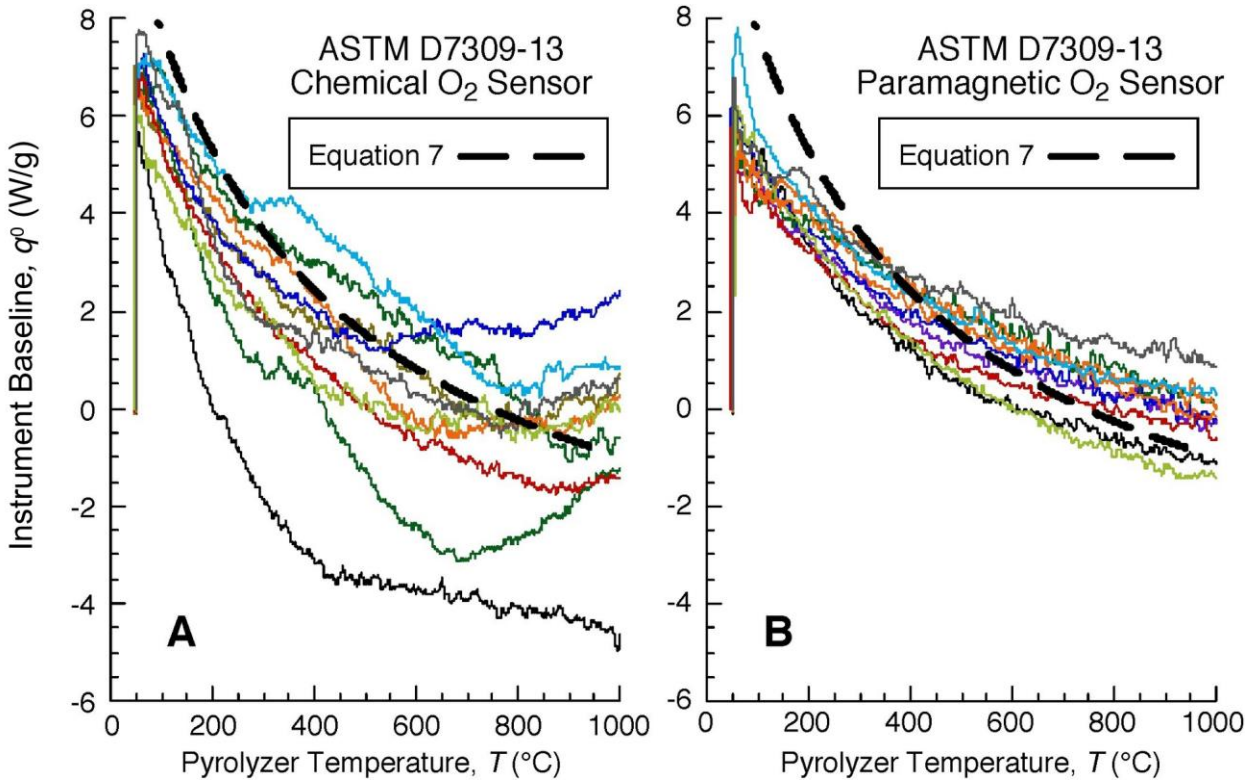

Figure 7. Replicate ASTM D7309-13 baseline measurements with chemical (A) and paramagnetic (B) oxygen sensors and Equation 7

Figure 8 shows the instrument baseline q^0 for 10 empty pan MCC experiments over the temperature range of controlled heating in Method A of ASTM D7309-19+ (Guo, Lyon, & Safronava, 2017) scaled to a spurious sample mass of 5 mg and heated at β = 1K/s from 50°C to 1000°C. Also shown in Figure 8, as a thick dashed curve, is the thermal baseline q_0 computed with Equation 10 using the properties in Table 1. Figure 8A shows that the magnitude of instrument thermal drift q^0 in ASTM D7309-19 (Method A), (ASTM International, 2019; ASTM International, 2021) is significantly less than q^0 of ASTM D7309-13 (Method A) (ASTM International, 2013) in Figure 7. However, random baseline fluctuations are still superimposed on the thermal drift during the test. Figure 8B shows q^0 of ASTM D7309-19 (Method A) (ASTM International, 2019; ASTM International, 2021) with O_2 measured using the paramagnetic oxygen analyzer. The total baseline drift over the course of the test is comparable to the chemical oxygen sensor in Figure 8, but the magnitude of the fluctuations is reduced for the paramagnetic oxygen analyzer.

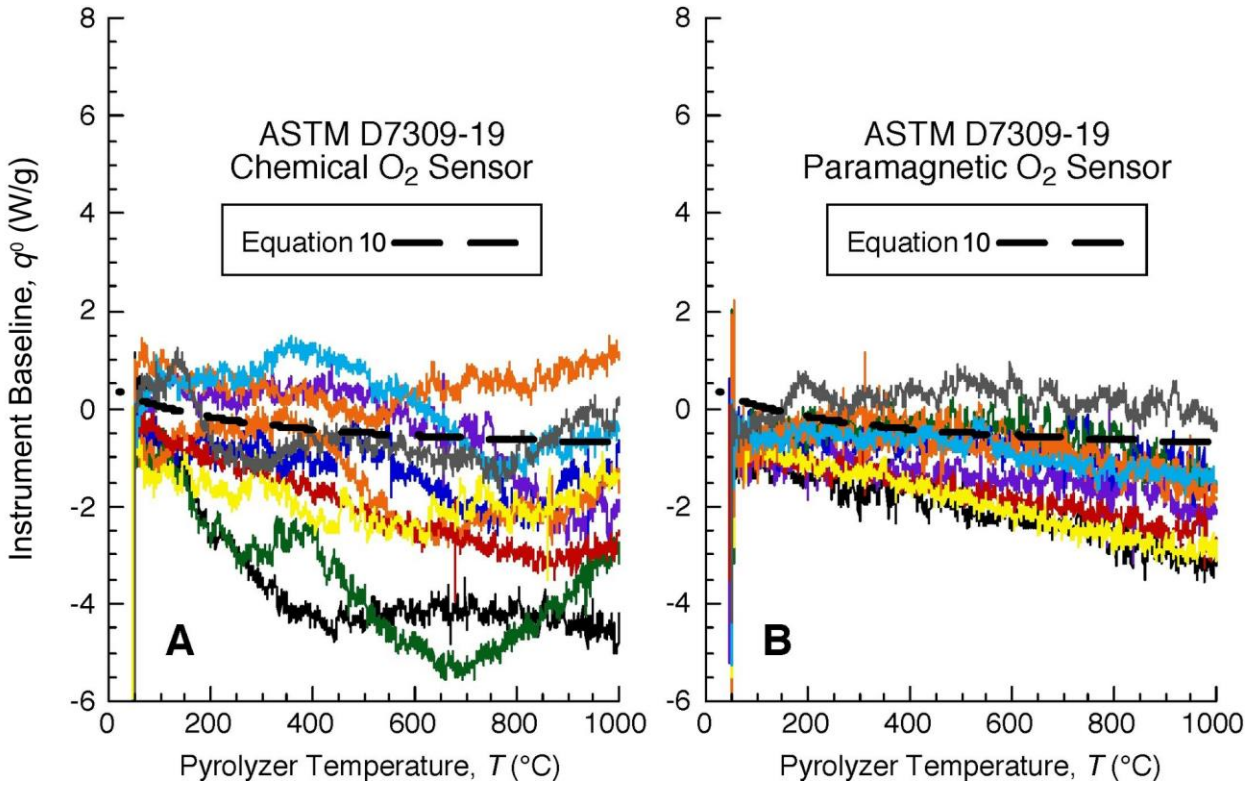

Figure 8. Replicate ASTM D7309-19 blank measurements with chemical (A) and paramagnetic (B) oxygen sensors and Equation 10

5.1.2 Oxidative pyrolysis baselines (Method B)

Figure 9 shows four replicate instrument baselines q^0 for a spurious 5 mg specimen computed for Method B of ASTM D7309-13. Also plotted in Figure 9 are the thermal baselines q_0 calculated using Equation 15 and 16 from p_1 and p_2 at the temperature limits of controlled heating, 373K (100°C) and 1373K (1100°C). In each case, the fluctuations of the instrument baseline q^0 are periodic with reversing slopes, while the thermal baseline q_0 is monotonically positive and the slope is proportional to the difference between the pyrolyzer temperature and the final (combustor) temperature.

Figure 10 shows the same instrument baseline data plotted in Figure 9 but analyzed using the updated $q(t,T)$ calculation (Equation 9) in ASTM D7309-19+ (ASTM International, 2019). In contrast to the instrument baselines q^0 of Method A in Figure 7 and Figure 8 that trend downward with increasing temperature, the Method B instrument baselines q^0 trend upward with increasing temperature and asymptotically approach constant values as the pyrolyzer temperature approaches the final/combustor temperature. Comparing Figure 9 and Figure 10 shows that the magnitude of the fluctuations in q^0 are comparable for the two versions of the standard but the magnitude of the drift is greater for D7309-19+.

The average computed thermal baselines q_0 in Figure 8A and Figure 10 are summarized in Figure 11 for D7309-19+ (ASTM International, 2019; ASTM International, 2021).

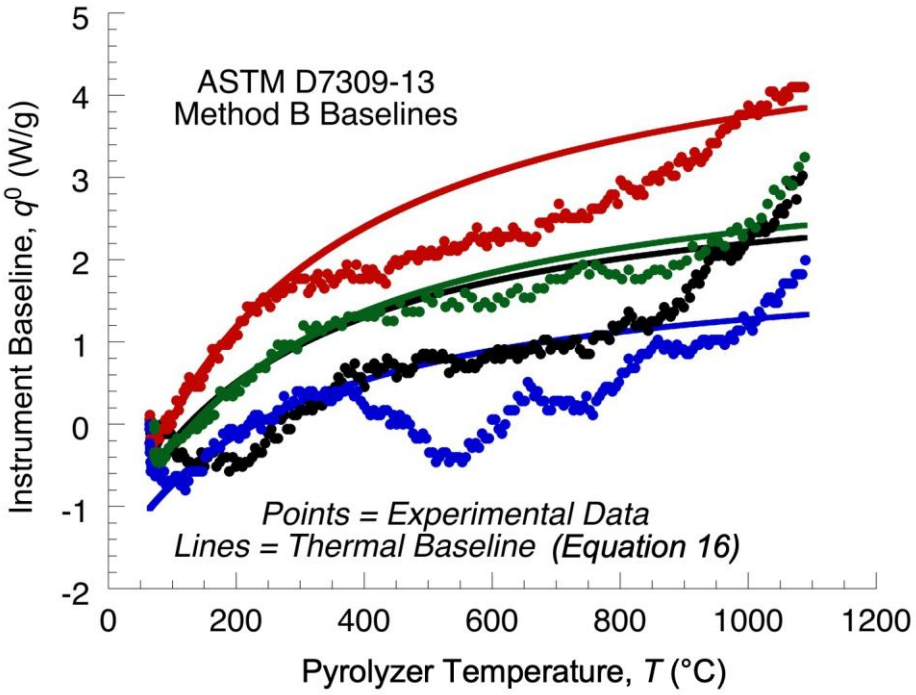

Figure 9. Instrument q^0 and thermal q_0 baselines for blank tests in Method B of ASTM D7309-13

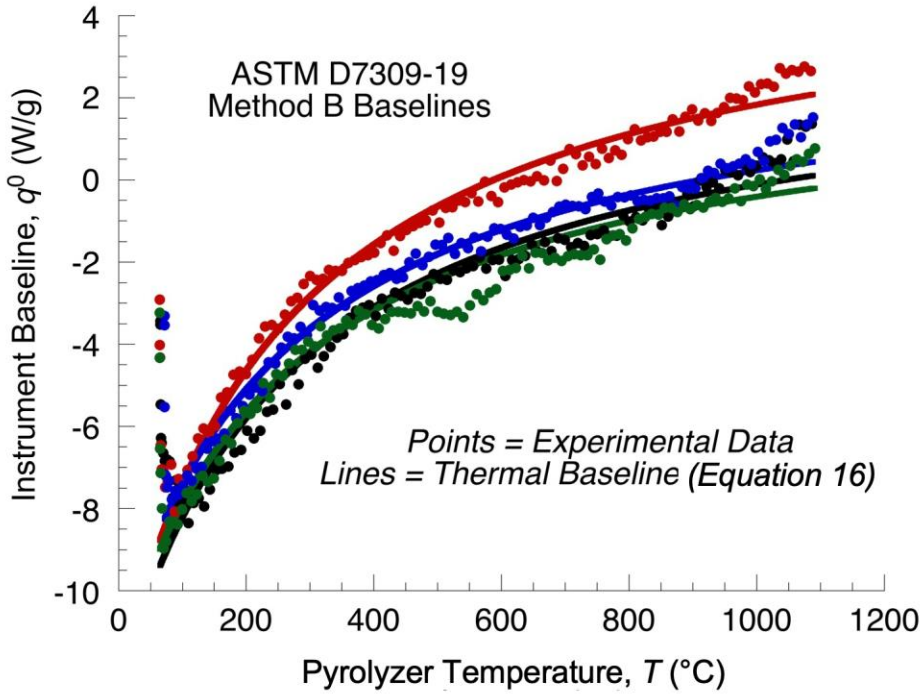

Figure 10. Instrument q^0 and thermal q_0 baselines for blank tests in Method B of ASTM D7309-19

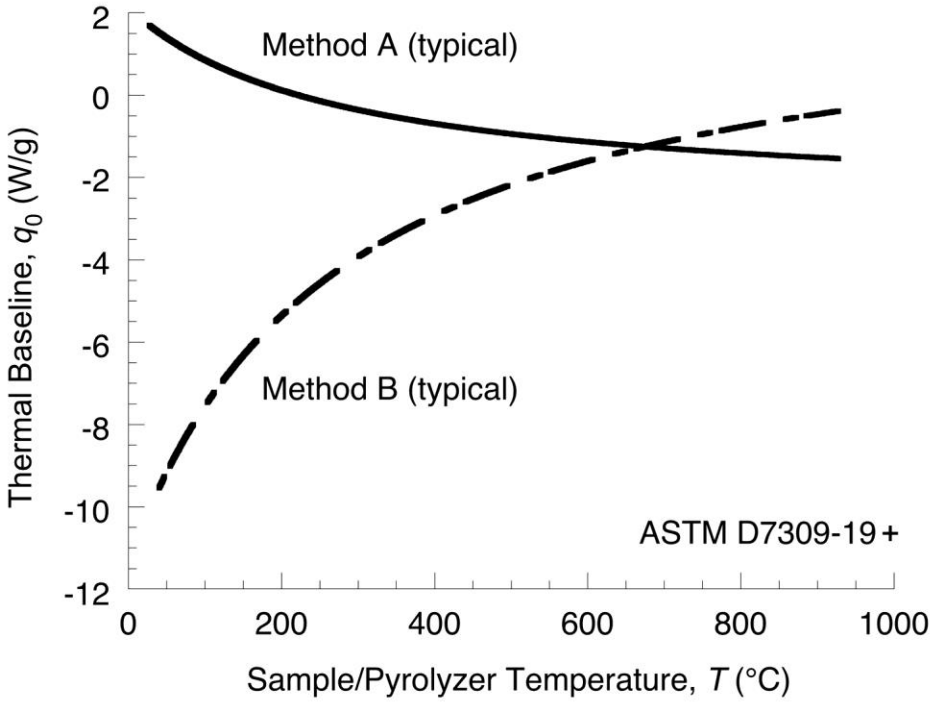

Figure 11. Average thermal baselines q_0 for Method A and Method B of ASTM D 7309-19

5.1.3 Baseline fluctuations

Figure 8 showed that high frequency (1 Hz) sampling noise and low frequency (mHz) chemical oxygen sensor fluctuations are superimposed on the monotonic thermal drift of Method A and Method B in the blank (q^0) tests of the instrument baseline. Figure 12 shows that the deviation of the instrument baselines q^0 of Figure 8A from the best-fit thermal baselines q_0 for these data, $\delta q^0 = q^0 - q_0$, can be positive or negative and have significant curvature and inflections over the typical 200°C to 400°C range of sample heat release.

High frequency sampling noise can be removed from the δq^0 of Figure 12, and $q(t,T)$ in general, using data smoothing techniques that preserve the trends in the low frequency q^0 fluctuations during baseline drift (Chambers, Cleveland, Kleiner, & Tukey, 1983). Figure 13 shows the result of locally weighted scatter plot smoothing (Chambers, Cleveland, Kleiner, & Tukey, 1983) of a single δq^0 from Figure 12 with a 20K data window. A central moving average of time-based data for a period of 20K/β seconds produces similar results. The solid line passing through the high frequency scatter is the locally weighted least squares regression curve. The smoothed data has approximately the same root mean squared deviation of q^0 from the thermal baseline q_0, as the noisy data, $\langle \delta q_0 \rangle = 0.5$ W/g and $\langle \delta q_0 \rangle = 0.7$, respectively, indicating that the observed limit of detection in ASTM D7309-19 (ASTM International, 2019; ASTM International, 2021) is determined by the low frequency fluctuations of q^0 associated with the chemical oxygen sensor.

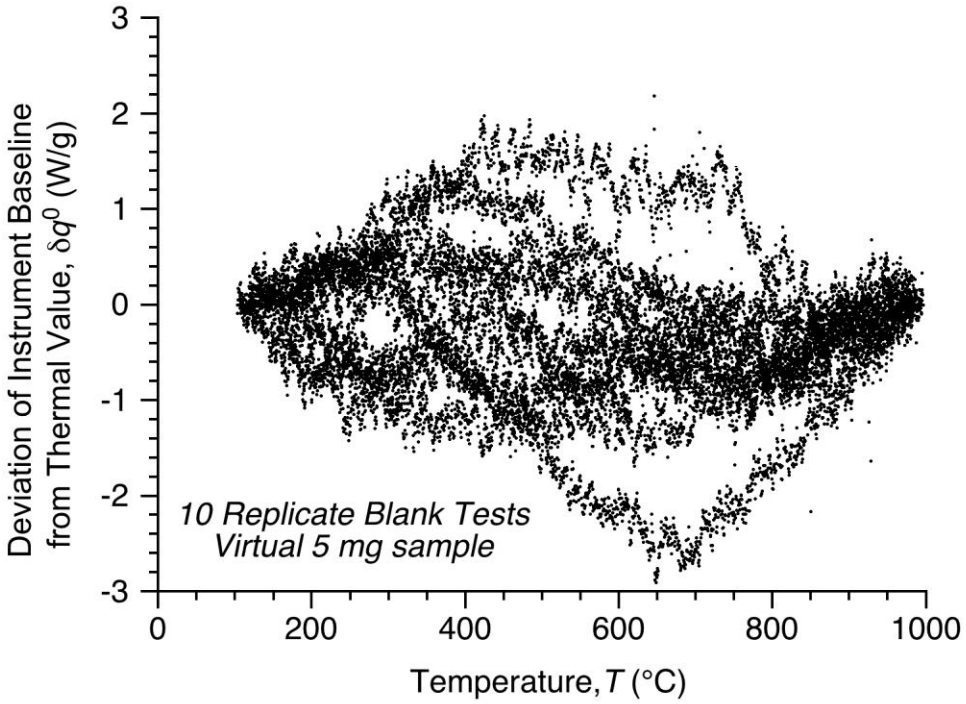

Figure 12. Low frequency non-thermal baseline fluctuations $\delta q^0 = q^0 - q_0$ with superimposed high frequency sampling noise

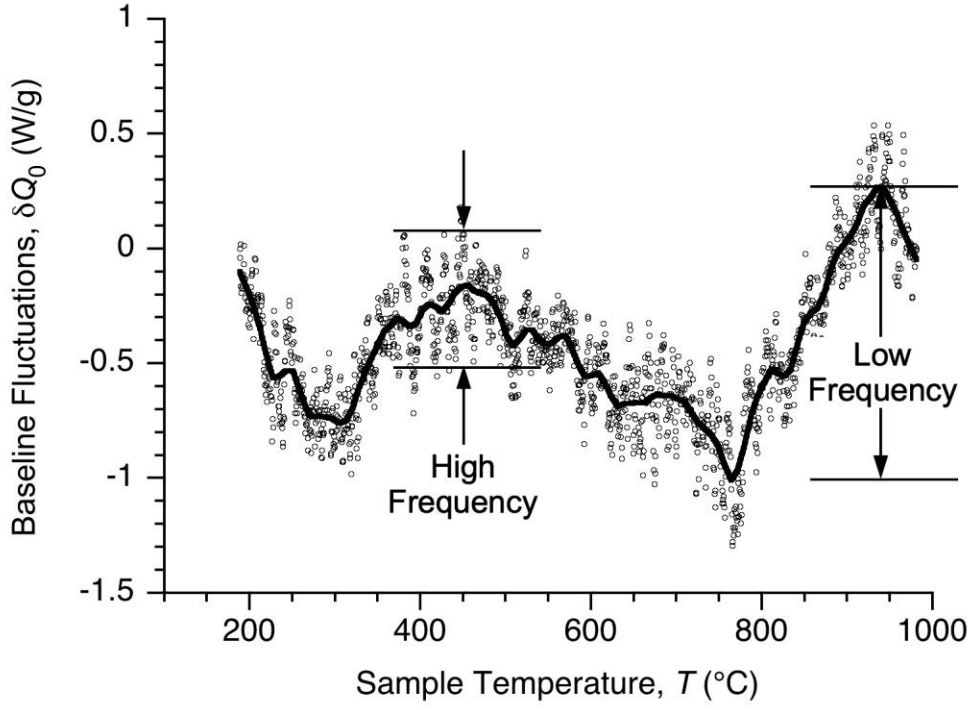

Figure 13. Reduction of sampling noise for a single δq^0 of Figure 12 using a smoothing routine

5.1.4 Sensitivity of baseline fit to p_1 and p_2

The uncertainty in two-point baseline fits associated with the choice of points, $p_1 = \{q_1, T_1\}$ and $p_2 = \{q_2, T_2\}$ was studied for the empty pan, instrumental baseline experiments in Figure 7A by selecting $p_1 = \{T_1, Q_1\}$ over a range of temperatures, T_1 = 100, 150, 200, 250 and 300°C, and $p_2 = \{T_2, Q_2\}$ over a range of temperatures, T_2 = 600, 700, 800, and 900°C. These temperature ranges bracket the typical heat release range 300°C-600°C shown as the shaded area in Figure 14. The perturbations of T_1 and T_2 result in 20 combinations of p_1, p_2 as illustrated in Figure 14 for $q(T)$ of an empty sample pan in ASTM D7309-19 (Method B) (ASTM International, 2019; ASTM International, 2021). For comparison purposes, these same perturbations were analyzed using a linear baseline fit between p_1 and p_2 using Equation 19. Figure 14 also shows the Method B baseline calculated using Equation16 for p_1 = {-8W/g, 373K} and p_2 = {-2W/g, 873K}. A linear baseline between these same p_1 and p_2 was computed using Equation15 and Equation 19, and is also shown in Figure 14.

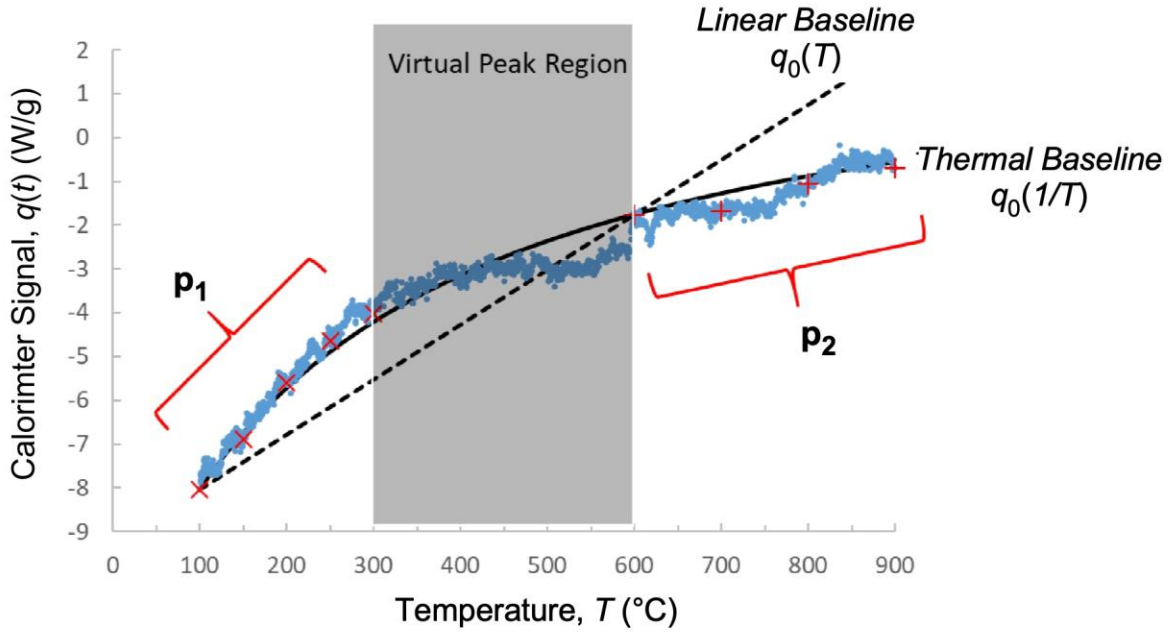

Figure 14. Thermal baseline and linear baseline fits to ASTM D7309-19 (Method B) for p_1 = (-8W/g, 373K) and p_2 = (-2W/g, 873K)

The total root-mean-square (RMS) deviation of measured q^0 from computed q_0 between p_1 and p_2, for the 20 perturbations, $\langle \delta q_0 \rangle$, was calculated for each of the two-point baseline models ($1/T$ and T) and used as an overall goodness of fit indicator. An additional calculation was performed to

estimate the baseline deviation at the maximum heat release rate, $\langle \delta q_{0,\text{peak}} \rangle$, which is expected to be in the temperature range, 573K-873K (300°C-600°C).

The average deviation $\langle \delta q_0 \rangle$ ± one standard deviation from the thermal (1/T) baseline for the 20 perturbations of p_1, p_2 is listed in Table 2. These results are for the single representative Method B test of Figure 13, and a single representative Method A test from Figure 7A or Figure 8A when $q(t,T)$ is calculated by ASTM D7309-13 (ASTM International, 2013) or ASTM D7309-19 (ASTM International, 2019; ASTM International, 2021). The average deviation of the linear (T) fit between the same 20 perturbations of p_1 and p_2 is also listed in Table 2. It is seen that the mean deviation of q^0 from q_0 for the thermal (1/T) and linear (T) fits are similar for Method A, but the (1/T) fit is significantly better than the (T) fit for Method B of the 2019 and later versions of the standard.

Table 2. Average RMS deviation of thermal (1/T) and linear (T) baseline fits to a single q^0

		Thermal Baseline (1/*T*)		**Linear Baseline (*T*)**	
Method	**D7309-**	**$\langle \delta q_0 \rangle$ (W/g)**	**$\langle \delta q_{0,\text{peak}} \rangle$ (W/g)**	**$\langle \delta q_0 \rangle$ (W/g)**	**$\langle \delta q_{0,\text{peak}} \rangle$ (W/g)**
A	2013	0.63±0.14	0.59±0.16	0.94±0.19	0.72±0.43
A	2019+	0.82±0.19	0.77±0.28	0.74±0.17	0.66±0.20
B	2013	0.42±0.08	0.46±0.11	0.41±0.08	0.44±0.08
B	2019+	0.39±0.02	0.47±0.05	0.90±0.25	0.84±0.47

Figures 5-9 and Figures 11-13 show that the instrument baseline q^0 is a superposition of high frequency sampling noise and low frequency fluctuations on the monotonic thermal drift of both Method A and Method B. In order to assess the effect of these random fluctuations on the overall error of the baseline fits, the mean and standard deviation of the RMS deviations of q^0 from q_0 for the empty sample pan (q^0) experiments in Figures 7A, 8A, 9, and 10 were calculated and summarized in Table 3. As in Table 2, the mean deviation of the instrument baseline q^0 from the thermal q_0 baseline for the reciprocal (1/T) and linear (T) temperature models is similar for Method A, but the reciprocal temperature (1/T) fit is significantly better than the linear temperature (T) fit for Method B of the 2019 (ASTM International, 2019) and later (ASTM International, 2021) versions of the standard.

Table 3. Average RMS deviation of thermal (1/*T*) and linear (*T*) baseline fits to multiple q^0

		Thermal Baseline (1/*T*)		**Linear Baseline (*T*)**	
Method	**D7309-**	$\langle \delta q_0 \rangle$ **(W/g)**	$\langle \delta q_{0,\,peak} \rangle$ **(W/g)**	$\langle \delta q_0 \rangle$ **(W/g)**	$\langle \delta q_{0,\,peak} \rangle$ **(W/g)**
A	2013	0.55±0.19	0.53±0.22	0.91±0.35	0.75±0.31
A	2019+	0.64±0.21	0.63±0.26	0.59±0.21	0.53±0.18
B	2013	0.35±0.17	0.33±0.16	0.36±0.12	0.35±0.11
B	2019+	0.39±0.10	0.36±0.11	0.80±0.24	0.74±0.26

Table 2 and Table 3 summarize the effect of 20 different choices of p_1 and p_2 on the goodness-of-fit of the two-point baseline models (1/*T* and *T*) from a single experiment (Table 2) and ten replicate experiments (Table 3), for two versions of the standard (2013 (ASTM International, 2013) and 2019 (ASTM International, 2019; ASTM International, 2021)), and the two methods therein (A and B). The RMS deviation of q^0 from the fitted value q_0 is less than 1 W/g in all cases, which is significantly less than the deviation of q^0 from zero (Figures 2, 3, and 5 and Figures 7 through 10), which justifies the use of baseline correction for all experiments.

5.2 Sample measurements

A perturbation analysis was conducted to investigate the extent to which the choice of p_1 and p_2 affects the corrected specific heat release rate $Q(t)$ and its time integrated value, the specific heat release h_c (e.g., Figure 5). An analysis was also conducted to compare the specific heat release h_c and FGC (Lyon, Safronava, Crowley, & Walters, 2021) for global p_1 and p_2 at the limits of controlled heating versus local p_1 and p_2 in the vicinity of the heat release event, as illustrated in Figure 5. Both the global and local baseline correction procedures include random q^0 fluctuations, but local selection of p_1 and p_2 seeks to maximize h_c (i.e., the grey area in Figure 2), so that h_c is biased towards higher values when the specific heat release rate $Q(t)$ is small (see Figure 5).

5.2.1 Sensitivity of specific heat release h_c to p_1 and p_2

Figure 15 is a plot of the uncorrected calorimeter signal, $q = Q + q^0$, versus temperature for a low heat release phenolic thermosetting resin (Phenolic A) used in aircraft interiors obtained by Method A of ASTM D7309-19+ (ASTM International, 2019; ASTM International, 2021), for which the fluctuations have reversed the normal downward trajectory of q^0 in a Method A test.

Visual inspection of Figure 15 suggests that heat is released from around 200°C to 900°C (ΔT = 700K) during the temperature scan at β = 1K/s. In order to test the effect of various choices of p_1 and p_2 on the specific heat release (h_c) at (ΔT = 700°C) and outside (ΔT > 700°C) the visually estimated range of heat release, five samples of Phenolic A were tested at temperature intervals: $\Delta T = T_2 - T_1$ = 700, 750, 800, 850, 900, 950 and 975°C, with T_1 and T_2 falling within the range of the rectangles before and after the heat release event as indicated in Figure 15.

Figure 16 shows mean values of time integrated $Q(t)$ for the 5 phenolic samples as h_c, versus the ΔT for the thermal (1/T) baseline correction. In each case, ΔT equals (700°C) or exceeds the visual range of sample heat release. Error bars are one standard deviation of the mean of 5 samples. It is seen that the average value, h_c = 6.7±0.4 kJ/g is within the uncertainty of the individual values over the entire range of ΔT, which indicates that the thermal (1/T) baseline method of Equations 15 and 16 is relatively insensitive to the choice of p_1 and p_2 for this extremely low heat release aircraft thermosetting resin.

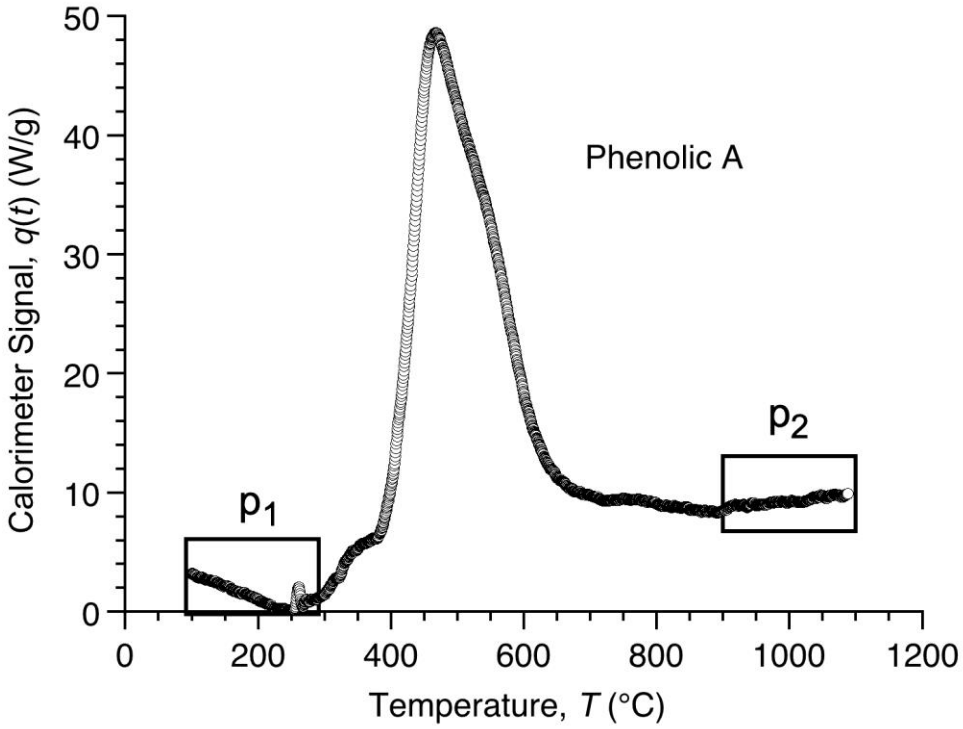

Figure 15. Specific heat release rate in Method A of ASTM D7309-19 vs temperature for phenolic showing ranges of p_1 and p_2

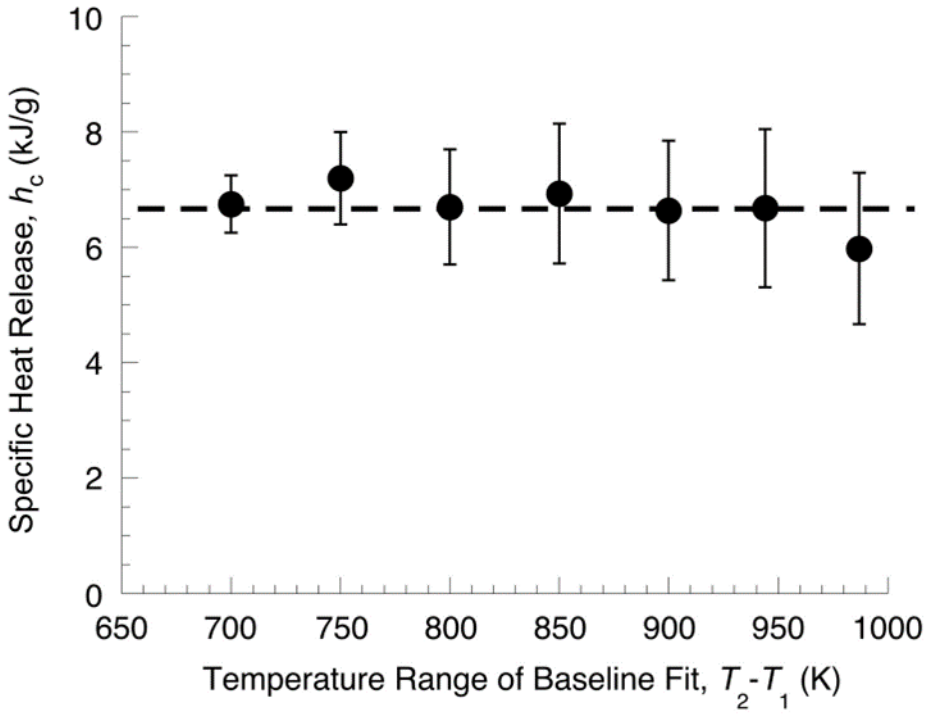

Figure 16. Specific heat release h_c of phenolic A vs temperature range T_2-T_1 of baseline fit in ASTM D7309-19+, Method A

5.2.2 Sensitivity of specific heat release h_c and FGC to method of baseline correction

Figure 17 is a plot of the specific heat release h_c of 300 combustible materials after global baseline correction for T_1 and T_2 at the temperature limits of controlled heating *versus* h_c of the same 300 materials obtained by local baseline correction at temperatures in the vicinity of the heat release event (see Figure 5). As mentioned previously, local linear or polynomial baseline fitting by a skilled operator seeks to maximize h_c, as evidenced by a slope of less than unity in Figure 17 for 1131 replicate tests of 300 samples. The global h_c using the (1/T) and (T) models is highly correlated with the local h_c, and the RMS deviation of the global and local values of specific heat release, δh_c, is less than 1 kJ/g, as shown in the legend.

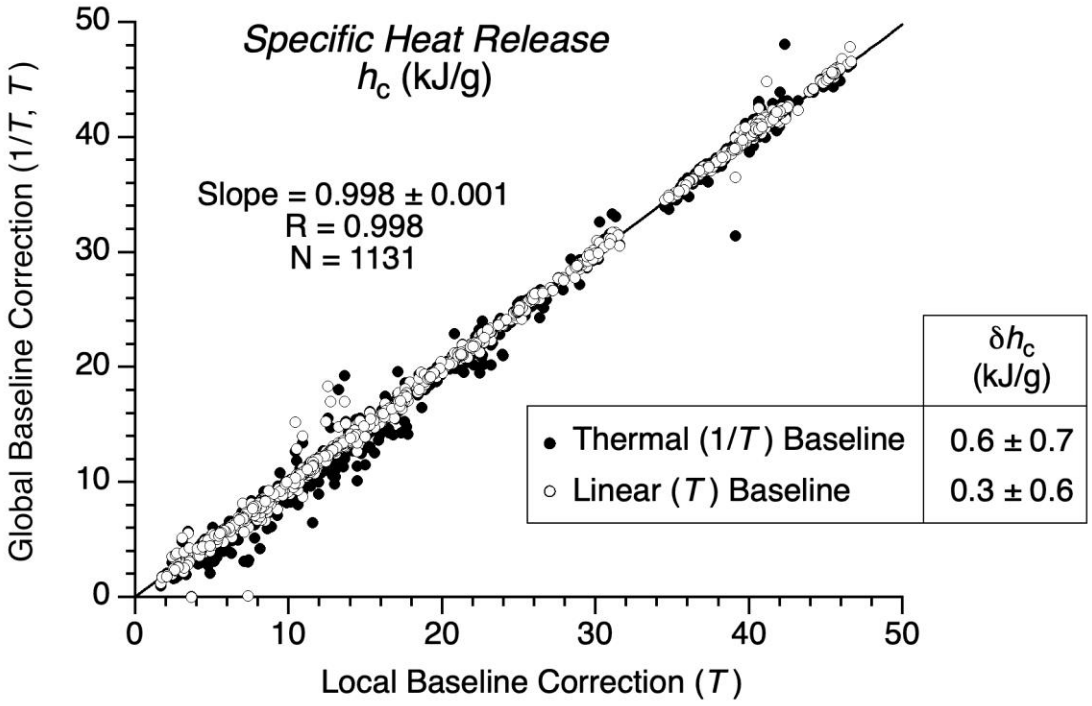

Figure 17. Specific heat release h_c after global vs local baseline correction

Figure 18 shows $Q(t)$ of Figure 4 on the left ordinate and its time integral at temperature T, $h(T)$, on the right ordinate versus temperature T on the abscissa. The maximum value of specific heat release is $h(T_2) = h_c = 6.6$ kJ/g. Temperatures at 5% ($T_{5\%}$) and 95% ($T_{95\%}$) of h_c are used to calculate the Fire Growth Capacity/FGC (Lyon, Safronava, Crowley, & Walters, 2021; Lyon, Safronava, Crowley, & Walters, 2020; Safronava, Lyon, & Walters, 2020),

$$FGC = \frac{h_c}{T_{5\%}-T_0} + \frac{h_c}{T_{95\%}-T_{5\%}} = \frac{6600\ J/g}{676K-298K} + \frac{6600\ J/g}{1011K-676K} = 83\ \frac{J}{g-K} \qquad (21)$$

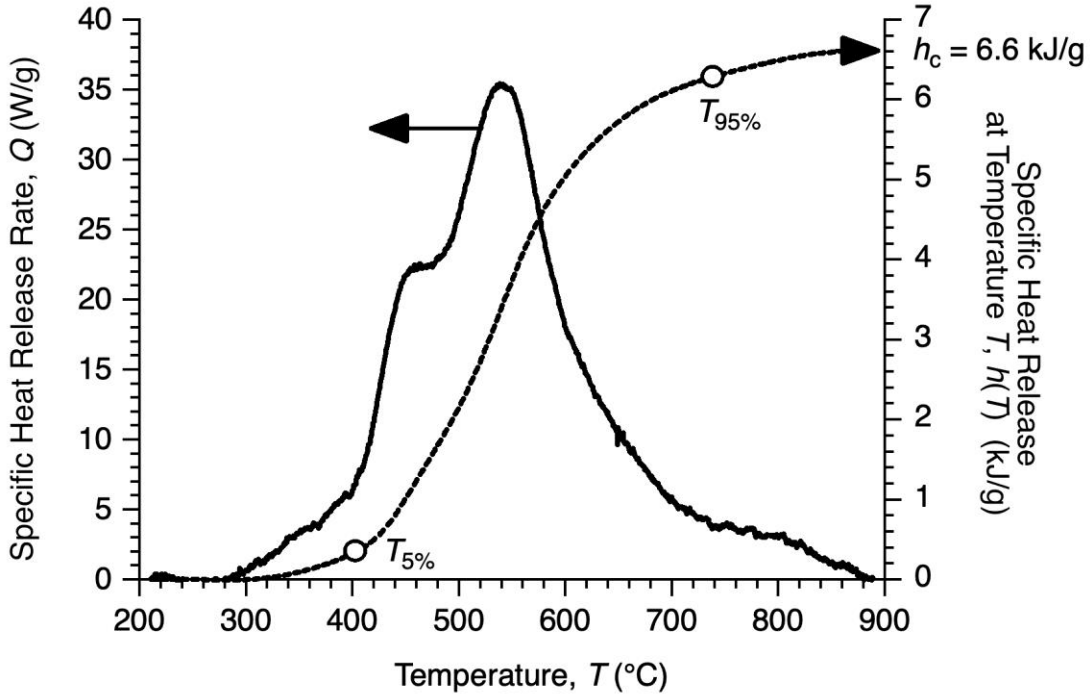

Figure 18. Baseline corrected $Q(t)$ and time integral $h(T)$ vs temperature $T(t)$ measured in Method A of ASTM D7309-19

Figure 19 compares the FGC (Lyon, Safronava, Crowley, & Walters, 2021) after global baseline correction using the $1/T$ and T baseline models at the limits of controlled heating, and local baseline correction using the T model at the limits of detectable heat release, as illustrated by the dotted line between p_1 and p_2 in Figure 5. The FGC by the global methods with $1/T$ and T baseline models is highly correlated with FGC from the local method using the T baseline model, and the difference in the RMS deviation of the global values from the local values, δFGC, is about 10 J/g-K, as shown in the legend of Figure 19.

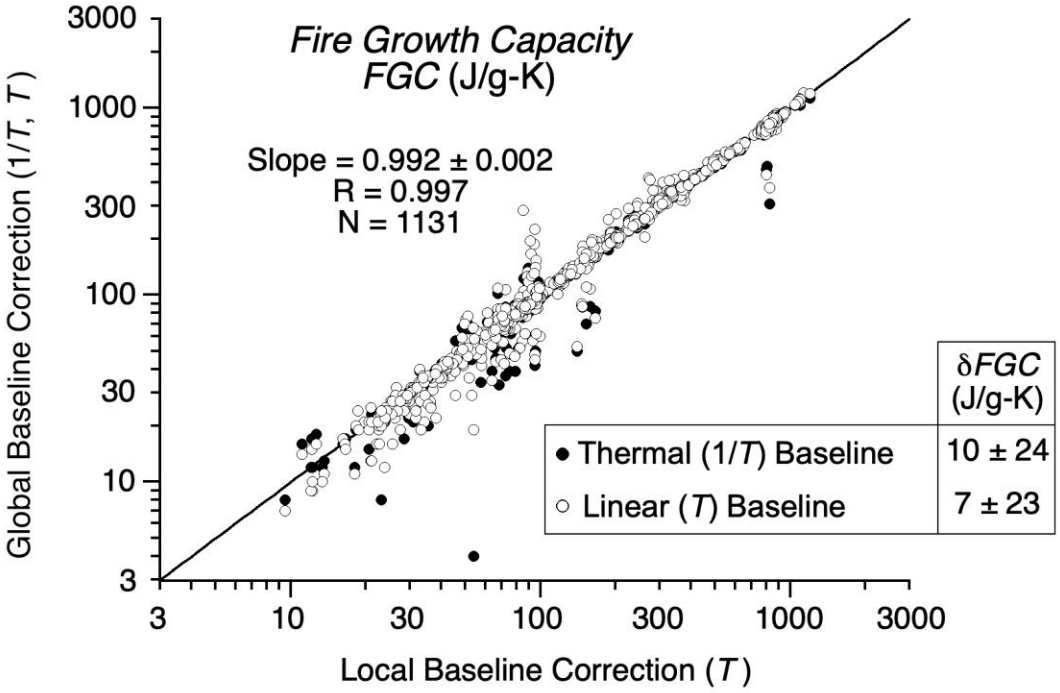

Figure 19. Fire growth capacity after global vs local baseline correction

5.3 Polystyrene standards

5.3.1 Anaerobic pyrolysis ASTM D7309-21 (Method A)

Figure 20 shows the uncorrected calorimeter signal, $q = Q + q^0$, for PS in Method A of D7309-19+ over the temperatures of controlled heating and the approximation $q_0 = q^0$ as per Figure 2 and Equations 15 and 16. The ordinate $q(t,T)$ has been expanded 100X to more clearly show the points $p_1 = \{q_1, T_1\}$ and $p_2 = \{q_2, T_2\}$ used to compute the thermal baseline $q_0(T)$. The total baseline drift Δq_0 during heat release of PS is approximately 2 W/g.

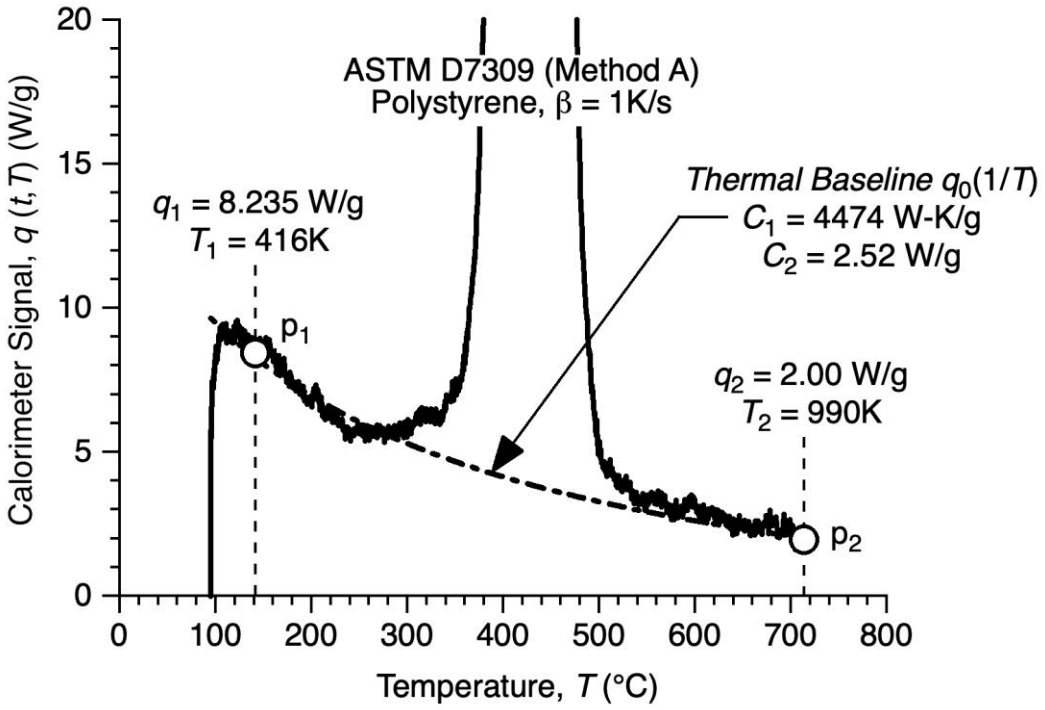

Figure 20. Two-point fit of $q_0(1/T)$ for polystyrene tested in Method A of ASTM D7309-19

Table 4. Specific heat release (h_c) and FGC of polystyrene for three baseline correction methods

Polystyrene	**Parameter**	**Baseline Correction Method**			**Average All Methods**
		Global 1/*T*	**Global *T***	**Local *T***	
Styron 665	h_c (kJ/g)	40.67	40.63	40.50	40.60
N = 79	Std. Dev.	2.80	2.86	2.59	2.75
	C.O.V. (%)	6.9	7.0	6.4	6.8
	FGC (J/g-K)	855	853	870	859
	Std. Dev.	81	91	56	76
	C.O.V. (%)	9.5	10.7	6.4	8.9
Various PS*	h_c (kJ/g)	41.10	41.01	40.84	40.98
N = 146	Std. Dev.	2.44	2.44	2.22	2.37
	C.O.V. (%)	5.9	6.0	5.4	5.8
	FGC (J/g-K)	851	852	863	855
	Std. Dev.	76	80	59	72
	C.O.V. (%)	8.9	9.4	6.8	8.4

**Styron 612, Styron 665, Styron 666, 8 x 10^6 Da, 1 x 10^6 Da, Polysciences PS.*

5.3.2 Oxidative pyrolysis (Method B)

Figure 21 is a plot of the calorimeter signal, $q = Q + q^0$ for 3 mg sample of PS pyrolyzed in the aerobic environment of Method B of the 2019+ version of the standard. The ordinate is expanded 100X to better show the points $p_1 = \{q_1, T_1\}$ and $p_2 = \{q_2, T_2\}$ used in Equations 15 and 16 to calculate the thermal baseline $q_0(1/T)$ over the temperatures of controlled heating. The result is shown as the dashed curve connecting these points. Also shown in Figure 21 is the measured heating rate during the oxidative pyrolysis test. The heating rate is uncontrolled near 400°C because the sample ignites in the aerobic environment. To prevent ignition in the Method B test, the heating rate or sample mass should be reduced so that the pyrolysis gases do not reach their lower flammability limit and auto ignite in the hot pyrolyzer.

Figure 22 shows three replicate measurements of corrected specific heat release rate, $Q(t) = q(T) - q^0 \approx q(T) - q_0$ for polystyrene under oxidative pyrolysis (Method B) using the 2019+ (ASTM International, 2019; ASTM International, 2021) version of the ASTM standard to compute Q. The variability of the maximum specific heat release rate, Q_{max}, is probably due to ignition of the

sample in the aerobic environment. Time integration of $Q(t)$ in Figure 22 gives, h_c^0 = 42.2 ± 0.2 kJ/g. This net calorific value of heat release is not significantly different at the 95% confidence level from the value, h_c^0 = 40.1 ± 0.8 kJ/g reported for Method B in (ASTM International, 2013) and later versions of the standard (ASTM International, 2019; ASTM International, 2021). This despite the greater accuracy of the heat release rate calculation in the 2019+ version of the standard (ASTM International, 2019; ASTM International, 2021) and the higher fidelity of the thermal baseline $q_0(1/T)$ to q^0 than the linear baseline $q_0(T)$ (Lyon, Walters, Stoliarov, & Safronava, 2014).

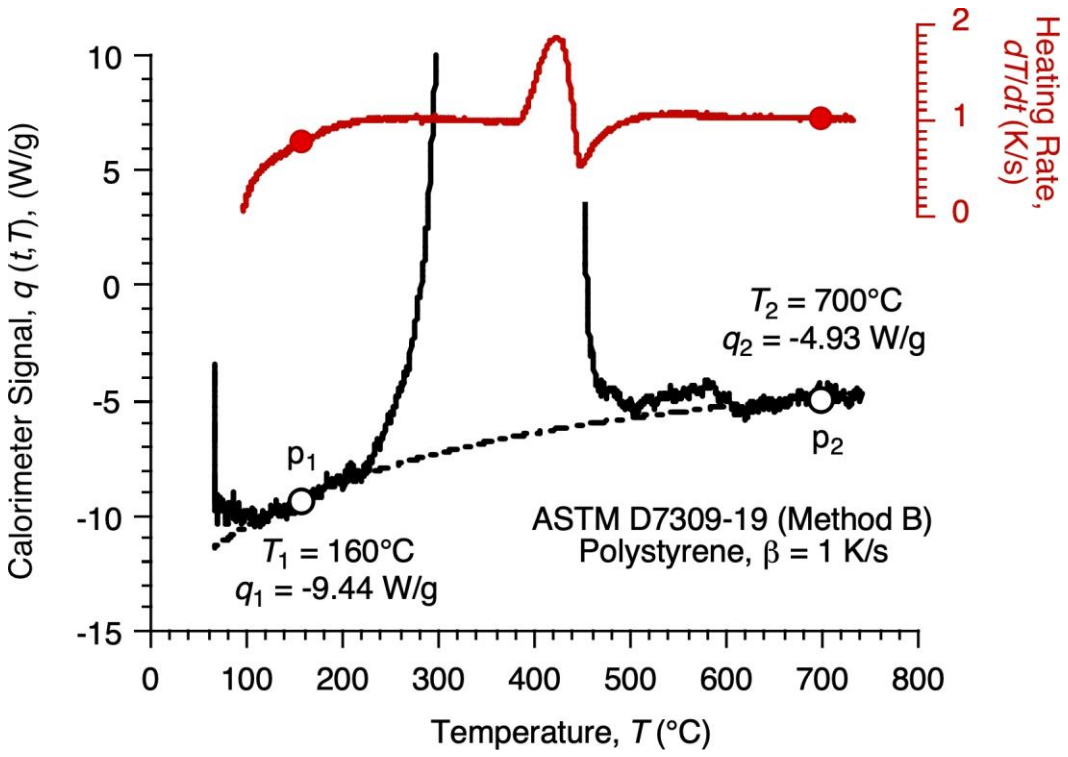

Figure 21. Two-point fit of $q_0(1/T)$ for polystyrene in Method B of ASTM D7309-19

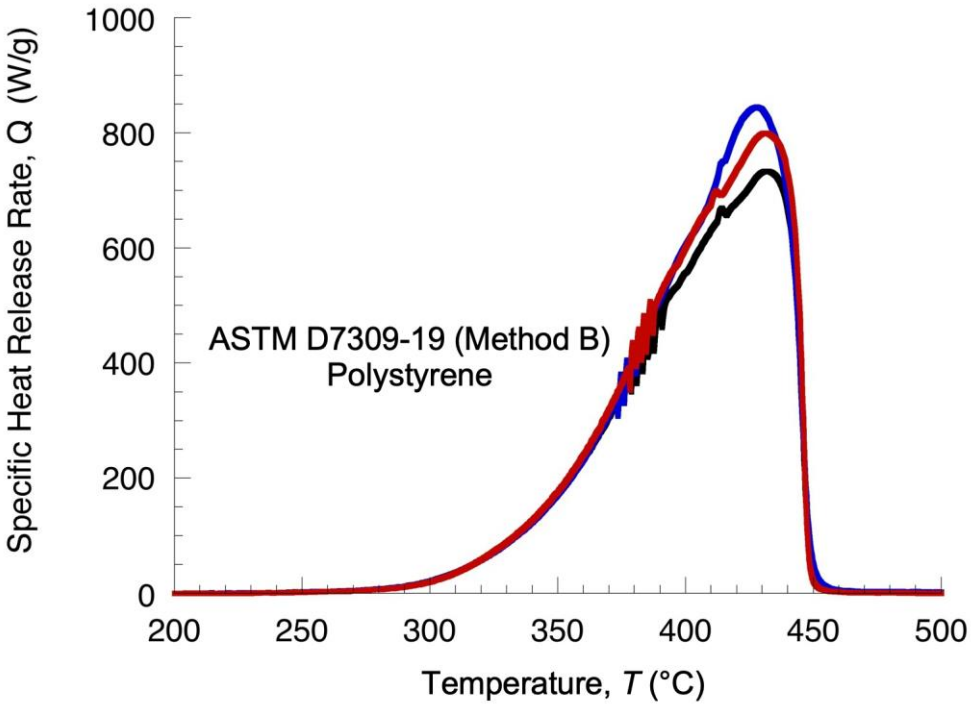

Figure 22. Baseline corrected $Q(t)$ histories for PS in Method B of ASTM D7309-19

6 Performance characteristics of ASTM D7309-19+

6.1 Resolution of MCC

The minimum heat release rate that can be resolved in ASTM D7309-19 and later versions of the standard is limited by the resolution of the chemical oxygen sensor, which is specified to be 0.1% of full scale (100% O_2), i.e., $X_{O_2}^{min} = 10^{-3}$ (m^3 O_2)/(m^3 O_2). The resolution of the commercial MCC in ASTM D7309-19+ is therefore,

$$\delta q^0 = (X_{O_2}^{\ 0})(F_0)(X_{O_2}^{\ min})(\rho_{O_2})(E)$$

$$= \left(0.2\ \frac{m^3\ O_2}{m^3\ (N_2+O_2)}\right)\left(1.67x10^{-6}\ \frac{m^3\ (N_2+O_2)}{s}\right)\left(10^{-3}\ \frac{m^3\ O_2}{m^3\ O_2}\right)\left(1.4\ \frac{kg\ O_2}{m^3\ O_2}\right)\left(13.1\ \frac{MJ}{kg\ O_2}\right)$$

$$= 6\ \text{mW}$$

$$\approx\ 1\ \text{W/g for 5 mg sample.}$$

6.2 Limits of detection

6.2.1 Specific heat release rate, $Q(t)$

According to ASTM International (2021), the limit of detection (LOD) or smallest value of $Q(t)$ that can be reliably detected is 3.3 times the instrument resolution,

- LOD = $3.3\langle\delta q^0\rangle$ = (3.3)(1 W/g) ≈ 3 W/g (Method A and Method B)

6.2.2 Specific heat release (h_c) and net calorific value (h_c^0)

The uncertainty in the specific heat release, h_c, is the uncertainty in the time integrated value of the instrument baseline q^0. Assuming, $q^0 \approx q_0(1/T)$ and integrating Equation 16 over the temperatures of controlled heating in the absence of a heat release event,

$$\langle\delta h_c\rangle = h_c - \frac{1}{\beta}\int_{T_1}^{T_2} q_0(T)dT = 0 - \frac{C_1}{\beta}\ln\left[\frac{T_2}{T_1}\right] + \frac{C_2}{\beta}(T_2 - T_1) \quad (22)$$

The temperature range of controlled heating is approximately, T_1 = 373K to T_2 = 1170K. Substituting empirical values for Method A, $C_{1,A}$ = 1294 W-K/g, $C_{2,A}$ = 2.61 W/g, and Method B, $C_{1,B}$ = -3877 W-K/g, $C_{2,B}$ = -2.85 W/g, into Equation 22 gives $\langle\delta h_c\rangle$ = 600 J/g for Method A, and $\langle\delta h_c^0\rangle$ = 2187 J/g for Method B at β = 1 K/s for a spurious 5 mg sample. From these values and the definition in (ASTM International, 2021),

- LOD of h_c = $3.3\langle\delta h_c\rangle$ = (3.3)(0.6 kJ/g) ≈ 2 kJ/g (Method A)
- LOD of h_c^0 = (3.3)(2.2 kJ/g) ≈ 7 kJ/g (Method B)

7 Conclusions

The MCC calorimeter signal $q(t,T)$ in the absence of a sample, q^0, is the sampling noise and analyzer fluctuations superimposed on a global $1/T$ thermal baseline that is intrinsic to the normal operation of the instrument. The magnitude of the instrument baseline q^0 depends on how the calorimeter signal $q(t,T)$ is calculated in the different versions of the standard (2013 or 2019), while the temperature dependence of q^0 depends on the method used (A or B) and the oxygen sensor stability (chemical or paramagnetic). The temperature dependence of the instrument baseline, $q_0(1/T)$ for all versions, methods, and oxygen sensors examined in this study is described by Equation 16,

$$q_0(1/T) = \frac{C_1}{T} - C_2$$

The coefficients C_1 (W-K/g) and C_2 (W/g) of the thermal baseline are specific values that depend on the sample mass and heating rate in the test, and therefore must be evaluated for each test using the coordinates of two points in the $q(t,T)$ history, one of which is before, $p_1 = \{T_1, q_1\}$, and one of which is after, $p_2 = \{T_2, q_2\}$, the heat release event as per Equations 17 and 18,

$$C_1 = \frac{q_1 - q_2}{T_2 - T_1} T_1 T_2 \qquad\qquad C_2 = \frac{q_1 T_1 - q_2 T_2}{T_2 - T_1}$$

An empirical two-point baseline that is appropriate for local baseline correction is a linear interpolation between $p_1 = \{T_1, q_1\}$ and $p_2 = \{T_2, q_2\}$ as described by Equation 19,

$$q_0(T) = c_1 + c_2(T - T_1)$$

The linear coefficients c_1 and c_2 also depend on the sample mass and heating rate and must be evaluated using the coordinates of p_1 and p_2 as per Equation 20,

$$c_1 = q_1, \qquad c_2 = \frac{q_2 - q_1}{T_2 - T_1}$$

The specific heat release rate $Q(t)$ is the time dependent part of the calorimeter signal $q(t,T)$, while the baselines $q_0(1/T)$ and $q_0(T)$ approximate the temperature-dependent instrument baseline, q^0. The relationship between the specific heat release rate of the sample $Q(t)$, the thermal baseline and the calorimeter signal $q(t,T)$ is given by Equation 15,

$$Q(t) = q(t,T) - q_0(T)$$

Integrating the specific heat release rate of the sample $Q(t)$ over time between the temperatures of heat release (T_1, T_2) provides the specific heat release of the sample, h_c, with a detection limit of about 2 kJ/g in Method A.

The reciprocal ($1/T$) and linear (T) thermal baseline (q_0) approximations to q^0 are relatively insensitive to the choice of p_1 and p_2, as long as they are outside the temperatures of heat release but within the temperatures of controlled heating. However, superimposed on this thermal drift is high frequency (Hz) sampling noise that can be mitigated using a moving average over a period of $20K/\beta$ seconds.

Three strategies for baseline correction were investigated:

1. Global Method: A reciprocal $q_0(1/T)$ or linear $q_0(T)$ thermal baseline model is fit to the calorimeter signal q between temperatures at the start (T_1 global) and end (T_2 global) of controlled heating (i.e., when the instantaneous heating rate exceeds 90% of the programmed value, $dT/dt \geq 0.9\beta$). Subtraction of q_0 from q provides Q, h_c and FGC.

2. Local Method: A reciprocal $q_0(1/T)$ or linear $q_0(T)$ thermal baseline model is fit to the calorimeter signal q between temperatures at the start (T_1 local) and end (T_2 local) of the heat release event as determined by visual or algorithmic inspection of q. Subtraction of q_0 from q provides Q, h_c and FGC.
3. Global/Local Method: Successive application of the global and local methods of baseline correction in a two-step procedure appears to be robust and amenable to automation in a limited study (see Figure 6).

Site-built MCCs conforming to ASTM D7309-21 using the chemical oxygen sensor supplied with commercial instruments and operated by a skilled user have the following performance characteristics:

- MCC Resolution = 6 mW (≈ 1 W/g based on a 5 mg sample).
- LOD of specific heat release rate, Q = 3 W/g for a 5 mg sample (Method A or Method B).
- LOD of Specific Heat Release, h_c = 2 kJ/g (Method A).
- LOD of Net Calorific Value, h_c^0 = 7 kJ/g (Method B).
- Uncertainty of Fire Growth Capacity, δFGC ≈ 10 J/g-K.

8 References

ASTM International. (2013). *Standard Test Method for Determining Flammability Characteristics of Plastics and Other Combustible Solid Materials Using Microscale Combustion Calorimetry ASTM D7309-13.* Retrieved from https://www.astm.org/standards/d7309

ASTM International. (2018). *Standard Test Method for Decomposition Kinetics by Thermogravimetry, ASTM E1641-18.* Retrieved from https://www.astm.org/e1641-18.html

ASTM International. (2019, May). *Standard Test Method for Determining Flammability Characteristics of Plastics and Other Combustible Solid Materials Using Microscale Combustion Calorimetry ASTM D7309-19.* Retrieved from https://webstore.ansi.org/Standards/ASTM/astmd730919

ASTM International. (2021). *Standard Test Method for Determining Flammability Characteristics of Plastics and Other Combustible Solid Materials Using Microscale*

Combustion Calorimetry ASTM D7309-21. Retrieved from https://standards.globalspec.com/std/14393088/astm-d7309-21

ASTM International. (2021). *Standard Test Method for Enthalpy Measurement Validation of Differential Scanning Calorimeters, ASTM E2253-21.* Retrieved from https://www.astm.org/e2253-21.html

Chambers, J., Cleveland, W., Kleiner, B., & Tukey, P. (1983). *Graphical Methods for Data Analysis.* Boston, MA: Duxbury Press.

Gibson, R., Simmons, M., Stittt, E., Horsburgh, L., & Gallen, R. (2022). Selection of Formal Baseline Correction Methods in Thermal Analysis. Retrieved from https://onlinelibrary.wiley.com/doi/10.1002/ceat.202100120

Guo, H., Lyon, R., & Safronava, N. (2017). Accuracy of Heat Release Measured in Microscale Combustion Calorimetry. *Journal of Testing and Evaluation*, *46*(3), 1090-1098.

Guo, H., Lyon, R., & Safronava, N. (2017). *Accuracy of the Heat Release Measured in Microscale Combustion Calorimetry, FAA Technical Note DOT/FAA/TC-TN17/5.* Retrieved from https://www.fire.tc.faa.gov/pdf/TC-TN17-45.pdf

Lyon, R., Safronava, N., Crowley, S., & Walters, R. (2020). *A Physical Basis for Comparing Flammability of Aircraft Cabin Materials Using a Microscale Combustion Calorimeter.* Retrieved from https://www.fire.tc.faa.gov/pdf/tc20-35.pdf

Lyon, R., Safronava, N., Crowley, S., & Walters, R. (2021). A Molecular-level Fire Growth Parameter. Retrieved from https://doi.org/10.1016/j.polymdegradstab.2020.109478

Lyon, R., Walters, R., Stoliarov, S., & Safronava, N. (2014). *Principles and Practice of Microscale Combustion Calorimetry.* Retrieved from https://www.fire.tc.faa.gov/pdf/tc-12-53.pdf

Safronava, N., Lyon, R., & Walters, R. (2020). *A Microscale Fire Test for Constituent Substitutions in Aircraft Cabin Materials.* Retrieved from https://www.fire.tc.faa.gov/pdf/tc20-30.pdf